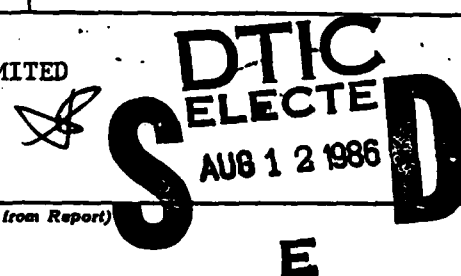


1

REPORT DOCUMENTATION PAGE		READ INSTRUCTIONS BEFORE COMPLETING FORM
1. REPORT NUMBER AFIT/CI/NR 86-82D	2. GOVT ACCESSION NO.	3. RECIPIENT'S CATALOG NUMBER
4. TITLE (and Subtitle) A Comparison of Nonlinear Filters for Orbit Determination and Estimation		5. TYPE OF REPORT & PERIOD COVERED THESIS/DISSERTATION
		6. PERFORMING ORG. REPORT NUMBER
7. AUTHOR(s) Daryl Gene Boden		8. CONTRACT OR GRANT NUMBER(s)
9. PERFORMING ORGANIZATION NAME AND ADDRESS AFIT STUDENT AT: University of Illinois		10. PROGRAM ELEMENT, PROJECT, TASK AREA & WORK UNIT NUMBERS
11. CONTROLLING OFFICE NAME AND ADDRESS AFIT/NR WPAFB OH 45433-6583		12. REPORT DATE 1986
		13. NUMBER OF PAGES 99
14. MONITORING AGENCY NAME & ADDRESS (if different from Controlling Office)		15. SECURITY CLASS. (of this report) UNCLAS
		15a. DECLASSIFICATION/DOWNGRADING SCHEDULE
16. DISTRIBUTION STATEMENT (of this Report) APPROVED FOR PUBLIC RELEASE; DISTRIBUTION UNLIMITED		
17. DISTRIBUTION STATEMENT (of the abstract entered in Block 20, if different from Report) E		
18. SUPPLEMENTARY NOTES APPROVED FOR PUBLIC RELEASE: IAW AFR 190-1		 LYNN E. WOLAVER 6A5FB Dean for Research and Professional Development AFIT/NR
19. KEY WORDS (Continue on reverse side if necessary and identify by block number)		
20. ABSTRACT (Continue on reverse side if necessary and identify by block number) ATTACHED.		

AD-A170 680

DTIC FILE COPY

A COMPARISON OF NONLINEAR FILTERS FOR ORBIT  
DETERMINATION AND ESTIMATION

BY

DARYL GENE BODEN

B.S., University of Colorado, 1972  
M.S., Air Force Institute of Technology, 1979

THESIS

Submitted in partial fulfillment of the requirements  
for the degree of Doctor of Philosophy in  
Aeronautical and Astronautical Engineering  
in the Graduate College of the  
University of Illinois at Urbana-Champaign, 1986



Urbana, Illinois

Accession For	
NTIS GRA&I	<input checked="" type="checkbox"/>
DTIC TAB	<input type="checkbox"/>
Unannounced	<input type="checkbox"/>
Justification	
By	
Distribution/	
Availability Codes	
Dist	Avail and/or Special
A-1	

UNIVERSITY OF ILLINOIS AT URBANA-CHAMPAIGN

THE GRADUATE COLLEGE

June 1986

WE HEREBY RECOMMEND THAT THE THESIS BY

DARYL GENE BODEN

ENTITLED A COMPARISON OF NONLINEAR FILTERS FOR ORBIT

DETERMINATION AND ESTIMATION

BE ACCEPTED IN PARTIAL FULFILLMENT OF THE REQUIREMENTS FOR  
DOCTOR OF PHILOSOPHY IN  
THE DEGREE OF AERONAUTICAL AND ASTRONAUTICAL ENGINEERING

Bruce A. Conway

Director of Thesis Research

Shi-ming Ye

Head of Department

Committee on Final Examination†

Bruce A. Conway

Chairperson

John S. Murphy

James Basan

for Phil Riebel

† Required for doctor's degree but not for master's.

## ACKNOWLEDGEMENTS

I wish to thank my advisor, Professor Bruce A. Conway, for his guidance and support throughout this research. Professor Conway's continued questioning of results and helpful suggestions provided great support and impetus during this program.

I also wish to thank Dr. Joseph J. F. Liu, Air Force SPACECOM/DOA, for suggesting this topic and for providing the observational data used in this research.

Finally, I wish to thank Dr. Paul J. Cefola, Charles Stark Draper Labs, for his numerous discussions and shared insight into the orbit determination problem.

ABSTRACT

This research compares the performance of three filters which have been applied to the problem of orbit determination using actual satellite tracking data obtained from ground based radars. The states estimated are the osculating classical orbital elements and the satellite ballistic coefficient. The dynamics used to propagate the state vector forward include the two-body acceleration plus perturbations due to atmospheric drag, zonal harmonics in the geopotential through  $J_2$ , and tesseral harmonics in the geopotential through  $J_{44}$ . The atmospheric density model used is an exponential model that includes diurnal variations and variations in the decimeter solar flux. The observations used to update the state vector estimates are slant range, azimuth, and elevation relative to a radar site.

The three filters investigated in this research are a nonlinear least squares filter, an Extended Kalman filter, and a Gauss second order filter. Data are processed for three different satellites. The first is a high altitude (1000km at perigee), non-circular ( $e=0.015$ ), orbit. The second satellite orbit is a low altitude (250km at perigee), non-circular ( $e=0.01$ ), orbit. The final orbit is a low altitude (300km), nearly circular ( $e=0.0003$ ), orbit.

The filters are compared using four criteria: estimation errors, prediction errors, computer time of operation, and computer storage requirements. The Gauss second order filter is shown to provide a substantial improvement in orbit determination accuracy for satellites subject to significant perturbing accelerations.

## TABLE OF CONTENTS

	<u>Page</u>
LIST OF TABLES . . . . .	viii
LIST OF FIGURES . . . . .	ix
LIST OF SYMBOLS . . . . .	x
CHAPTER	
1. INTRODUCTION . . . . .	1
1.1. Problem Statement . . . . .	1
1.2. Assumptions . . . . .	5
1.3. Thesis Overview . . . . .	6
2. SYSTEM MODEL . . . . .	7
2.1. Introduction . . . . .	7
2.2. Dynamics . . . . .	7
2.3. Observations . . . . .	16
3. ESTIMATION THEORY . . . . .	19
3.1. Introduction . . . . .	19
3.2. Least Squares Filter . . . . .	21
3.3. Extended Kalman Filter (EKF) . . . . .	27
3.4. Second Order Filters . . . . .	32
4. OBSERVATIONAL DATA . . . . .	37
4.1. Introduction . . . . .	37
4.2. Epoch Values of the Satellite Orbits . . . . .	37
4.3. Data Summary . . . . .	40
5. RESULTS . . . . .	43
5.1. Introduction . . . . .	43
5.2. Estimation Errors . . . . .	44
5.3. Prediction Errors . . . . .	54
5.4. Computer Time of Operation . . . . .	71
5.5. Computer Storage Requirements . . . . .	73
6. CONCLUSIONS AND RECOMMENDATIONS FOR FUTURE WORK . . . . .	74
6.1. Conclusions . . . . .	74
6.2. Recommendations for Future Work . . . . .	77
LIST OF REFERENCES . . . . .	80

## APPENDICES

A. Functions and Coefficients for Tesseral Harmonics . . . . .	82
B. State Transition Matrix . . . . .	86
C. Second Order Terms for Filter Equations . . .	88
D. Radar Site Locations . . . . .	98
VITA . . . . .	99



## LIST OF TABLES

<u>Table</u>	<u>Page</u>
4-1. Epoch Values for the Test Case . . . . .	38
4-2. Epoch Values for Satellite 4507 . . . . .	39
4-3. Epoch Values for Satellite 10299 . . . . .	39
4-4. Epoch Values for Satellite 6633 . . . . .	40
4-5. Observational Data . . . . .	42
5-1. Estimation Residuals of the Test Case . . . . .	47
5-2. Estimation Residuals for Satellite 4507 . . . . .	48
5-3. Estimation Residuals for Satellite 4507 Using Reduced Order Filters . . . . .	50
5-4. Estimation Residuals for Satellite 10299 . . . . .	50
5-5. Effect of Bias Terms in the Gauss Filter for Satellite 10299 . . . . .	51
5-6. Estimation Residuals for Satellite 6633 . . . . .	52
5-7. Effect of Bias Terms in the Gauss Filter for Satellite 6633 . . . . .	52
5-8. Computer Time of Operation (sec) . . . . .	72
5-9. Computer Storage Requirements (k of memory) . . . . .	73
A-1. Inclination Functions $F_{lmp}$ . . . . .	82
A-2. Eccentricity Functions $G_{lpq}$ (e) . . . . .	84
A-3. Geopotential Coefficients . . . . .	85
D-1. Radar Site Locations . . . . .	98

## LIST OF FIGURES

<u>Figure</u>	<u>Page</u>
5-1. Slant Range Prediction Errors for Satellite 4507 . . . . .	55
5-2. Azimuth Prediction Errors for Satellite 4507 .	56
5-3. Elevation Prediction Errors for Satellite 4507 . . . . .	57
5-4. Slant Range Prediction Errors Using Reduced Order Filters . . . . .	59
5-5. Azimuth Prediction Errors Using Reduced Order Filters . . . . .	60
5-6. Elevation Prediction Errors Using Reduced Order Filters . . . . .	61
5-7. Slant Range Prediction Errors for Satellite 10299 . . . . .	64
5-8. Azimuth Prediction Errors for Satellite 10299	65
5-9. Elevation Prediction Errors for Satellite 10299 . . . . .	66
5-10. Slant Range Prediction Errors for Satellite 6633 . . . . .	68
5-11. Azimuth Prediction Errors for Satellite 6633 .	69
5-12. Elevation Prediction Errors for Satellite 6633 . . . . .	70

## LIST OF SYMBOLS

$a$	semi-major axis
$\underline{a}_D$	acceleration due to atmospheric drag
$\underline{a}_p$	perturbing acceleration
$Az$	azimuth
$B$	ballistic coefficient
$B(t-)$	filter gain bias matrix
$\underline{b}_d$	dynamic bias vector
$\underline{b}_m$	observation bias vector
$C_{\ell m}$	geopotential coefficients
$e$	eccentricity
$El$	elevation
$F$	linearized dynamics matrix
$f$	satellite true anomaly
$\underline{f}$	system dynamics vector
$F_{\ell mp}(i)$	inclination functions for the geopotential
$F_{10.7}$	decimeter solar flux
$G_{\ell pq}(e)$	eccentricity functions for the geopotential
$H$	atmospheric scale height
$H$	linearized observation matrix
$h$	altitude above the Earth
$\underline{h}$	system observation model
$i$	inclination
$I$	identity matrix

$I_n$	Bessel functions of order $n$
$J_n$	zonal coefficients of the geopotential
$J_{lm}$	tesseral coefficients of the geopotential
$K$	filter gain matrix
$L$	geocentric latitude
$M$	mean anomaly
$n$	satellite mean motion
$P$	state covariance matrix
$p$	semi-latus rectum of orbit
$P_n$	Legendre polynomials of order $n$
$p(\underline{x}, t)$	probability density function of state vector
$Q$	process noise matrix
$R$	measurement noise matrix
$R$	Earth's mean equatorial radius
$\underline{R}$	position vector of radar site
$r$	distance of satellite from center of Earth
$\underline{r}$	satellite position vector
$\underline{r}$	observation residuals
$r_p$	radius of perigee
$S_{lm}$	geopotential coefficients
$t$	time
$t_o$	epoch time
$u$	satellite argument of latitude
$v$	satellite velocity
$\underline{v}$	satellite velocity vector

$\underline{v}_a$	velocity of satellite with respect to the atmosphere
$\underline{v}_k$	additive noise in observations
$V_{l,m}$	l,m term of the geopotential
$v_p$	velocity of perigee
$W$	weighting matrix
$\underline{w}(t)$	additive noise in dynamics model
$\underline{x}$	filter state vector
$\underline{z}_c$	predicted value of observations
$\underline{z}_o$	actual value of observations
$\underline{\delta x}$	estimate of error in state vector
$\theta$	local sidereal time
$\mu$	Earth's gravitational constant
$\rho$	slant range
$\rho$	atmospheric density
$\psi$	angle between satellite and subsolar atmospheric bulge
$\Phi$	state transition matrix
$\Omega$	longitude of ascending node
$\omega$	argument of perigee
$\omega_e$	Earth's rotational velocity

## CHAPTER 1

### INTRODUCTION

#### 1.1. Problem Statement

The orbit determination problem consists of two basic parts; propagation of the state estimates forward in time and updating the state estimate based upon new measurements of parameters which are functions of the states. The problem is complicated by the following three factors. First, the initial state vector, the satellite's orbital elements, is not known exactly. Next, the dynamics model used to propagate the state forward is only an approximate model. Finally, the measurements are corrupted by noise.

The states to be estimated are the classical orbital elements and the ballistic coefficient of the satellite. These elements are:

- a - semi-major axis,
- e - eccentricity,
- i - inclination,
- $\Omega$  - longitude of ascending node,
- $\omega$  - argument of perigee,
- M - mean anomaly, and
- B - ballistic coefficient

The classical orbital elements were chosen due to their descriptive nature. The semi-major axis and eccentricity

determine the size and shape of the orbit. The inclination and longitude of ascending node describe the orientation of the orbital plane in inertial space. The argument of perigee describes the orientation of the orbit in the orbital plane. Finally, the mean anomaly locates the satellite within the orbit. The ballistic coefficient is also estimated since it is not known for many objects orbiting the Earth and its estimate can incorporate uncertainty in the atmospheric model.

The dynamics model used to propagate the state vector forward in time for a satellite must contain the two-body equations of motion and any perturbations which are considered significant. The method used in this work is a variation of parameters formulation of the equations of motion which are integrated using special perturbations theory. The perturbations include atmospheric drag, zonal terms  $J_2 - J_6$  in the geopotential, and tesseral terms  $J_{22} - J_{44}$  in the geopotential. Since no model is exact, there are errors in the equations of motion. These errors, called process noise, are modeled as zero-mean, white, Gaussian noise.

Similarly, the measurements used to update the states are not exact, but are corrupted by noise in the observation data. These errors are also modeled as zero-mean, white, Gaussian noise.

The problem of satellite orbit determination is a very important one which has received much attention in the literature. In this work we will compare the accuracy and efficiency of several different filters for orbit determination. Among previous researchers who have made such comparisons are Kolenkiewicz and Fuchs (1) and Myers (2). The standard for comparison is a batch, nonlinear, least squares filter. This method has been used for years and has proven to be accurate when applied to the problem of orbit determination for a large number of satellites in different orbits. Currently, the Air Force Space Command uses a nonlinear least squares filter for element set maintenance for all objects orbiting the Earth (3). These objects, including active payloads, rocket bodies, and satellite fragments, number over 5000. The other filters considered are all recursive filters. Shavers (4) compares the performance of batch and recursive filters for orbit determination. Among the advantages of recursive filtering are a state estimate based on the most recent data available and the lack of a need to store the data for batch processing. One type of recursive filter is the Extended Kalman Filter. The final type of filter is a second order filter, which derives its name from the inclusion of the second order terms from the Taylor series expansion used to linearize the filter dynamics and observation equations.



The second order terms occur in the dynamics, observations, and filter gain equations. Tapley and Choe (5) compared the performance of a second order filter with the performance of an Extended Kalman filter for interplanetary orbit determination. They investigated the effect of the second order terms in the dynamics, observations, and filter gain separately, concluding that the second order term in the filter gain resulted in the most significant improvement over the Extended Kalman filter. Taylor (6) calculated the magnitude of the bias terms in the dynamics and observations for the determination of an orbit of an Earth satellite. He concluded that inclusion of the observation bias terms should improve the filter performance, but that the inclusion of the dynamic bias terms should not alter filter performance. However, Taylor (6) did not verify or quantify the improvement due to second order terms as they were never employed in the filters he used. Athans, Wishner, and Bertolini (7) compared the performance of a second order filter to the performance of a first order filter when applied to the problem of estimating the position and velocity of a vertically falling body. They concluded that the second order filter yields superior performance when nonlinearities are significant. They also concluded that the major improvement was due to the bias correction term in the dynamics.

In this research the orbit determination accuracy and efficiency of two recursive filters, an iterated-extended Kalman filter (EKF) and a Gaussian second order filter (GSF) will be compared to that of a batch least squares filter (LSF). Actual observation data for satellites in three different types of orbits will be used. The Gaussian second order filter will be examined in greatest detail. Following the approach of Tapley and Choe (5), the effect of the second order terms in the dynamics, observations, and gain will be evaluated individually. The efficiency of the filters, expressed as computer time of operation and required storage, will be compared.

### 1.2 Assumptions

The assumptions made in this research are:

- a. The system dynamics are continuous with process noise modeled by zero-mean, white, Gaussian noise.
- b. The measurements are discrete and are corrupted by zero-mean, white, Gaussian noise.
- c. The process noise and measurement noise are uncorrelated.
- d. The satellite ballistic coefficient is an unknown constant.
- e. The most significant perturbing forces are due to atmospheric drag and the geopotential terms

$J_2 - J_6$  and  $J_{22} - J_{44}$ . All other forces may be neglected.

f. The satellites are considered to be non-maneuvering.

### 1.3. Thesis Overview

The purpose of this thesis is to compare the performance of various filters applied to the orbit determination problem. Chapter 2 is a description of the mathematical system dynamics model used to propagate the state vector forward and the observations used to update the estimates of the states.

Chapter 3 provides an overview of the estimation problem and a detailed description of each of the filter algorithms used in this research.

Chapter 4 describes the satellite orbits and the data used to compare the filter performance.

Chapter 5 presents the results obtained by the filters using actual observational data. Results are presented regarding estimation errors, prediction errors, computer storage requirements, and computer operation time.

Finally, Chapter 6 contains the conclusions of this research and recommendations for future work.

## CHAPTER 2

### SYSTEM MODEL

#### 2.1. Introduction

The propagation of the satellite state vector requires an accurate force model in the equations of motion and a means of integrating the equations of motion. The method used in this research is to express the equations of motion in terms of Gauss' variation of parameters equations. The equations of motion are then integrated numerically using the method of special perturbations.

In addition to the dynamics model, the mathematical relationship between the observations and states must be defined in order for the filters to process the data and update the estimates of the states. The observations used in this research are slant range ( $\rho$ ), azimuth (Az), and elevation (El) relative to the radar site.

#### 2.2. Dynamics

The equations of motion of a satellite orbiting the Earth are given by Newton's 2<sup>nd</sup> Law as:

$$\ddot{\underline{r}} + \frac{\mu}{r^3} \underline{r} = \underline{a}_p \quad 2.1$$

where:

$\underline{r}$  is the position vector of the satellite from the center of the Earth,

$\mu$  is the Earth's gravitational constant, and  $\underline{a}_p$  are the perturbing accelerations.

These equations can be integrated directly, an approach called Cowell's method, but this approach is rather slow and inefficient due to the large changes in the magnitudes of the components of the satellite position vector and velocity vector. An alternate approach, called the Variation of Parameters, takes advantage of the periodic nature of equation 2.1. If only the two-body system is considered, equation 2.1 becomes:

$$\ddot{\underline{r}} + \frac{\mu}{r^3} \underline{r} = \underline{0}. \quad 2.2$$

If the equations of motion are now written in terms of the classical orbital elements, a system of six first order differential equations result in which all the derivatives are equal to zero except for mean anomaly which is:

$$\dot{M} = n, \quad 2.3$$

where:

$$n = \sqrt{\mu/a^3}, \text{ the mean motion.}$$

Writing the perturbing accelerations in terms of the classical orbital elements, the system equations of motion become:

$$\dot{\underline{x}} = \underline{f}(\underline{x}(t), t) \quad 2.4$$

where:

$\underline{x}$  is the seven-component state vector containing the classical orbital elements and the satellite ballistic coefficient, and

$\underline{f}$  is the vector containing the perturbing accelerations and the mean anomaly rate (Eq. 2.3).

The perturbations most significant for low-Earth orbit determination are acceleration due to atmospheric drag and acceleration due to a non-spherical Earth. The mathematical model of acceleration due to atmospheric drag is:

$$\underline{a}_D = -B\rho v_a \underline{v}_a / 2 \quad 2.5$$

where:

$\underline{a}_D$  is the acceleration due to atmospheric drag,

$B$  is the satellite ballistic coefficient,

$\rho$  is the atmospheric density, and

$\underline{v}_a$  is the velocity of the satellite relative to the atmosphere.

The acceleration due to atmospheric drag must now be expressed in terms of the state vector,  $\underline{x}(t)$ . The approach used in this thesis is that developed by King-Hele (8).

The resulting variational equations for an oblate atmosphere with rotational velocity equal to the Earth's rotational velocity are:

$$\begin{aligned}
\dot{a} &= -\rho B F a^2 v^3 / \mu \\
\dot{e} &= \rho B F v (e + \cos(f)) \\
\dot{i} &= -\rho v r^2 \omega_e (F/\mu p)^{1/2} \sin(i) \cos^2(u/2) \\
\dot{\Omega} &= \rho v r^2 \omega_e (F/\mu p)^{1/2} \sin(u) \cos(u) \\
\dot{\omega} &= -\cos(i) \dot{\Omega}
\end{aligned}
\tag{2.6}$$

where:

$$F = (1 - r_p \omega_e \cos(i) / v_p)$$

$r_p$  is the radius of perigee,  
 $v_p$  is the velocity at perigee,  
 $f$  is the satellite true anomaly,  
 $u = \omega + f$ ,  
 $\omega_e$  is the Earth's rotational velocity, and  
 $p$  is the semi-latus rectum.

A major computational effort in calculating the perturbation due to atmospheric drag is in determining the density,  $\rho$ . The simplest atmospheric model assumes a spherically symmetric density which varies exponentially with altitude:

$$\rho = \rho_0 \exp(-(h - h_0)/H) \tag{2.7}$$

where:

$\rho_0$  is the density at  $h_0$ ,  
 $h$  is the altitude above the surface of the Earth,  
 $h_0$  is the reference altitude, and  
 $H$  is the scale height.

A more sophisticated model developed by Jacchia (9) includes a diurnal variation due to solar heating and variations in the decimeter solar flux,  $F_{10.7}$ . The model used in this research is the 1960 Jacchia model with modifications described in Reference 3. For this model the density for altitudes less than 700km is:

$$\rho = \rho_0 0.85 F_{10.7} [1 + 0.2375 (\exp(0.0102h) - 1.9) (1 + \cos(\psi))^3] \quad 2.8$$

where:

$$\log_{10} \rho_0 = -15.738 - 0.00368h + 6.363 \exp(-0.0048h),$$

$\rho$  is the density in slug/ft<sup>3</sup>,

$$F_{10.7} = 1.5 + 0.8 \cos(\pi d / 2010),$$

$d$  is the number of days since 31 Dec. 1957,

$h$  is the altitude above the surface of the Earth in nautical miles, and

$\psi$  is the angle between the satellite and the subsolar atmospheric bulge.

Above 700km the density is

$$\rho = 0.00504 F_{10.7} h^{-8} [1/8 (1 + \cos \psi)^3 (h^3 - 6 \times 10^6) + 6 \times 10^6] \quad 2.9$$

The density scale height,  $H$ , varies with altitude and is obtained from a stored table.

The other major perturbation affecting the motion of a satellite in a low-Earth orbit is caused by the



gravitational attraction of the non-spherical Earth. The perturbing potential due to the axially symmetric part of the Earth's gravitational field is (10):

$$F = (\mu/r) \sum_{n=2}^{\infty} J_n (R/r)^n P_n(\sin(L)) \quad 2.10$$

where:

the  $J_n$  are the zonal harmonic coefficients of the Earth's mass distribution,

$R$  is the Earth's mean equatorial radius,

$P_n$  are Legendre polynomials of degree  $n$ , and

$L$  is the geocentric latitude,  $\sin L = \sin i \sin(\omega + f)$ .

The perturbing acceleration may be determined from the potential function:

$$\underline{a}_p = \nabla F. \quad 2.11$$

A convenient coordinate frame for expressing the components of acceleration is the STW frame where:

$S$  is the component along the radius vector,

$T$  is perpendicular to  $S$  in the orbit plane in the direction of motion, and

$W$  is normal to the orbit frame so that the STW frame forms a right-hand coordinate set.

The components of the disturbing acceleration are then:

$$\begin{aligned} S &= \partial F / \partial r, \\ T &= (1/r) \partial F / \partial u, \text{ and} \\ W &= (1/r \sin(u)) \partial F / \partial i. \end{aligned} \quad 2.12$$

The components of the disturbing acceleration due to the first five terms ( $n=2, \dots, 6$ ) of the disturbing geopotential, eq. 2.9, are given by Merson (11):

$$S = (\mu/r^2) [(3/2)J_2(R/r)^2(3A^2-1) + 2J_3(R/r)^3(5A^3-3A) + (3/8)J_4(R/r)^4(35A^4-30A^2+3) + (3/4)J_5(R/r)^5(63A^5-70A^3+15A) + (7/16)J_6(R/r)^6(231A^6-315A^4+105A^2-5)], \quad 2.13$$

$$T = -(\mu/r^2) \sin i \cos u [3J_2(R/r)^2A + (3/2)J_3(R/r)^3(5A^2-1) + (5/2)J_4(R/r)^4(7A^3-3A) + (15/8)J_5(R/r)^5(21A^4-14A^2+1) + (21/8)J_6(R/r)^6(33A^5-30A^3+5A)], \quad 2.14$$

$$W = (\mu/r^2) \cos i [\text{bracketed term in eq. 2.14}]. \quad 2.15$$

where:

$$A = \sin(i) \sin(u)$$

$$J_2 = 1082.628 \times 10^{-6}$$

$$J_3 = -2.538 \times 10^{-6}$$

$$J_4 = -1.593 \times 10^{-6}$$

$$J_5 = -0.230 \times 10^{-6}$$

$$J_6 = 0.502 \times 10^{-6}$$

The values of the geopotential coefficients are those derived by Kozai (12).

Having expressed the perturbing acceleration in the STW coordinate frame the most convenient set of perturbation equations is the Gaussian form of the Lagrange planetary

perturbation equations:

$$\begin{aligned}
 \dot{a} &= (2/n)(1-e^2)^{1/2} [e \sin(f) S + (p/r) T] \\
 \dot{e} &= (1-e^2)^{1/2} / (na) [\sin(f) S + (\cos(f) \\
 &\quad + (e + \cos(f)) / (1 + e \cos(f))) T] \\
 \dot{i} &= r \cos(u) / (na^2 (1-e^2)^{1/2}) W \\
 \dot{\Omega} &= r \sin(u) / (na^2 (1-e^2)^{1/2} \sin(i)) W \\
 \dot{\omega} &= (1-e^2)^{1/2} / (nae) [-\cos(f) S \\
 &\quad + \sin(f) (1 + r/p) T] - \cos(i) \dot{\Omega} \\
 \dot{M} &= n + 1 / (na^2 e) [(p \cos(f) - 2er) S - (p+r) \sin(f) T]
 \end{aligned} \tag{2.16}$$

where  $S$ ,  $T$ , and  $W$  are given by eqs. 2.13-2.15.

Finally, eqs. 2.16 are combined with eqs. 2.6 to form the system equations of motion (eq. 2.4).

In addition to the zonal terms in the geopotential which vary with latitude, longitude dependent terms, called tesseral terms, in the geopotential can be included in the equations of motion. Kaula (13) derived an expression for the geopotential,  $V_{\ell m}$ , as a function of the classical orbital elements:

$$V_{\ell m} = (\mu/a) (R/a)^{\ell} \sum_{p=0}^{\ell} F_{\ell mp}(i) \sum_{q=-\infty}^{\infty} G_{\ell pq}(e) S_{\ell mpq}(\omega, M, \Omega, \theta), \tag{2.17}$$

where:

the  $F_{\ell mp}(i)$  are the inclination functions,  
the  $G_{\ell pq}(e)$  are the eccentricity functions,

$$S_{\ell mpq} = \begin{cases} C_{\ell m} & \ell-m \text{ even} \\ S_{\ell m} & \ell-m \text{ odd} \end{cases} \cos[(\ell-2p)\omega + (\ell-2p+q)M + m(\Omega-\theta)] + \begin{cases} S_{\ell m} & \ell-m \text{ even} \\ C_{\ell m} & \ell-m \text{ odd} \end{cases} \sin[(\ell-2p)\omega + (\ell-2p+q)M + m(\Omega-\theta)], \text{ and}$$

the  $C_{\ell m}$  and the  $S_{\ell m}$  are the geopotential coefficients.

The inclination functions, eccentricity functions, and the geopotential coefficients are given in Appendix A.

The variational equations of motion due to the tesseral terms in the geopotential can be calculated by applying Lagrange's planetary equations due to a disturbing potential:

$$\begin{aligned} \dot{a} &= (2/na) \frac{\partial V_{\ell m}}{\partial M}, \\ \dot{e} &= (1/na^2 e) [(1-e^2) \frac{\partial V_{\ell m}}{\partial M} + (1-e^2)^{1/2} \frac{\partial V_{\ell m}}{\partial \omega}], \\ \dot{i} &= 1/(na(1-e^2)^{1/2}) [\cot(i) \frac{\partial V_{\ell m}}{\partial \omega} - \csc(i) \frac{\partial V_{\ell m}}{\partial \Omega}], \\ \dot{\Omega} &= \csc(i)/(na^2(1-e^2)^{1/2}) \frac{\partial V_{\ell m}}{\partial i}, \\ \dot{\omega} &= (1-e^2)^{1/2}/(na^2 e) \frac{\partial V_{\ell m}}{\partial e} - \cot(i)/(na^2(1-e^2)^{1/2}) \frac{\partial V_{\ell m}}{\partial i}, \text{ and} \\ \dot{M} &= -(1-e^2)/(na^2 e) \frac{\partial V_{\ell m}}{\partial e} - 2/(na) \frac{\partial V_{\ell m}}{\partial a}. \end{aligned} \tag{2.18}$$

The tesseral harmonics are of small amplitude and to first order cause no secular variations in the state, causing only periodic variations in the classical orbital elements (10).

Two assumptions were made when determining the variations due to the tesseral harmonics. First, only the terms through  $V_{44}$  were included. The indices for the potential,  $V$ , are therefore  $\ell=2,3,4$  and  $m=1, \dots, \ell$ . The terms in the geopotential for  $m=0$  are the zonal variations and are included in equation 2.16. The second assumption is that the eccentricity is small and can be neglected in the variational equations for the tesseral harmonics.

Finally, equations 2.18 are combined with equations 2.16 and 2.6 to form the system equations of motion (eq. 2.4).

Other forces acting on the satellite, such as solar radiation or third-body gravitation due to the sun or the moon, are not included in the dynamics model. Errors caused by neglecting these forces, as well as errors in the dynamics model due to uncertainties in parameters such as atmospheric density and geopotential coefficients will be compensated for in the process noise matrix described in Chapter 3.

### 2.3. Observations

The observations used to update the estimate of the state vector are slant range, azimuth, and elevation relative to a radar site. A mathematical model must be provided which relates the observations,  $\underline{z}$ , to the states,

$\underline{x}$ , i.e.

$$\underline{z} = \underline{h}(\underline{x}(t), t). \quad 2.19$$

The approach used in this work is to first express the satellite position vector,  $\underline{r}$ , in terms of the state vector,  $\underline{x}$ , in the perifocal (PQW) coordinate system (14):

$$\underline{r} = r \cos(f) \hat{P} + r \sin(f) \hat{Q} \quad 2.20$$

where  $\hat{P}$  and  $\hat{Q}$  are unit vectors in the orbital plane;  $\hat{P}$  is in the direction of perigee and  $\hat{Q}$  is perpendicular to  $\hat{P}$  in the direction of motion.

The next step is to rotate the position vector from the perifocal frame to the geocentric equatorial coordinate (GEC) frame and then to the topocentric horizon coordinate (THC) frame (14):

$$\begin{aligned} [\underline{r}]_{\text{THC}} &= M_2 [\underline{r}]_{\text{GEC}} \\ &= M_2 M_3 [\underline{r}]_{\text{PQW}} \end{aligned} \quad 2.21$$

where:

$$\begin{aligned} M_3(1,1) &= \cos(\Omega) \cos(\omega) - \sin(\Omega) \sin(\omega) \cos(i) \\ M_3(1,2) &= -\cos(\Omega) \sin(\omega) - \sin(\Omega) \cos(\omega) \cos(i) \\ M_3(1,3) &= \sin(\Omega) \sin(i) \\ M_3(2,1) &= \sin(\Omega) \cos(\omega) + \cos(\Omega) \sin(\omega) \cos(i) \\ M_3(2,2) &= -\sin(\Omega) \sin(\omega) + \cos(\Omega) \cos(\omega) \cos(i) \\ M_3(2,3) &= -\cos(\Omega) \sin(i) \end{aligned}$$

$$M_3(3,1) = \sin(\omega) \sin(i)$$

$$M_3(3,2) = \cos(\omega) \sin(i)$$

$$M_3(3,3) = \cos(i)$$

$$M_2 = \begin{bmatrix} \sin(L) \cos(\theta) & \sin(L) \sin(\theta) & -\cos(L) \\ -\sin(\theta) & \cos(\theta) & 0 \\ \cos(L) \cos(\theta) & \cos(L) \sin(\theta) & \sin(L) \end{bmatrix}$$

$L$  is the geocentric latitude of the radar site,  
and

$\theta$  is the local sidereal time of the radar site.

With the position vector,  $\underline{r}$ , expressed in the THC frame, the slant range vector is now:

$$\underline{\rho} = \underline{r} - \underline{R} = \rho_s \hat{S} + \rho_E \hat{E} + \rho_z \hat{z} \quad 2.22$$

where  $\underline{R}$  is the position vector of the radar site on an oblate Earth in the THC frame. Finally, the observations,  $\underline{z}$ , can be expressed as functions of the slant range vector,  $\underline{\rho}$ .

$$\begin{aligned} \rho &= (\rho_s^2 + \rho_E^2 + \rho_z^2)^{1/2} \\ Az &= \sin^{-1}(\rho_E / (\rho_s^2 + \rho_E^2)^{1/2}) \\ El &= \sin^{-1}(\rho_s / \rho) \end{aligned} \quad 2.23$$

# CHAPTER 3

## ESTIMATION

### 3.1. Introduction

The primary purpose of estimation is to provide an estimate of the state vector,  $\underline{x}(t)$ , based on a system dynamics model,  $\underline{f}(\underline{x}(t), t)$ , and observations known to be corrupted by noise,  $\underline{z}(t)$ . For the orbit determination problem a continuous, nonlinear, systems model with errors modeled by white-Gaussian noise,  $\underline{w}(t)$ , is used with discrete measurements corrupted by white-Gaussian noise,  $\underline{v}(t)$ . The system equations are:

$$\dot{\underline{x}}(t) = \underline{f}(\underline{x}(t), t) + \underline{w}(t), \quad \underline{w}(t) = N(\underline{0}, Q), \quad 3.1$$

$$\underline{z}(t_k) = \underline{z}_k = \underline{h}_k(\underline{x}(t_k)) + \underline{v}_k \quad \text{and}$$

$$\underline{v}(t_k) = \underline{v}_k = N(\underline{0}, R). \quad 3.2$$

where:

$Q$  is a diagonal process noise matrix, and

$R$  is a diagonal measurement noise matrix.

Also,  $\underline{v}$  and  $\underline{w}$  are assumed to be independent.

One method of updating the state estimate with noisy observations is a batch least squares filter. This approach determines an estimate of the state that minimizes the sum of the squares of the residuals. A residual is defined to



be the value of the actual observation minus the predicted value based on the state estimate. The batch, least squares filter will provide the base-line filter for evaluating the performance of other filters considered in this research.

Two disadvantages of the least squares filter are first that it does not use information about the process noise to update the state. Second, it is a batch processor. This requires that sufficient data for an update must be stored prior to the update. Also, the current estimate of the state vector from the batch processor does not contain information based on the most recent data, but is based on the data prior to the last update.

A second class of filters considered in this research, called recursive filters, include process noise in their state estimates and provide a state estimate based on all of the data, up to and including the most recent observation. For a linear problem with zero-mean, white, Gaussian noise the optimal estimator is the Kalman filter (15). For the nonlinear problem, the Kalman filter may no longer provide the optimal estimate of the state; however, the extended Kalman filter has been successfully applied to several nonlinear problems described by Maybeck (16), Gelb (17), and Jazwinski (18) and will therefore be considered in this research. The extended Kalman filter is based on a first

order Taylor series expansion of equations 3.1 and 3.2 about the state estimate. Retention of second order terms in the expansions results in truncated and Gaussian forms of second order filters. Only the Gaussian form of the second order filter will be considered in this research.

The following sections provide a description of each of the filters investigated along with the algorithm used for updating each filter.

### 3.2. Least Squares Filter

The basic principle of the method of least squares is that the best estimate of the state vector is the estimate which minimizes the sum of the squares of the residuals. Define the residual to be

$$\underline{r} = \underline{z}_0 - \underline{h}(\underline{x}), \quad 3.3$$

where:

$\underline{z}_0$  are the actual observations.

Since the actual value of the state,  $\underline{x}$ , is not known,  $\underline{h}(\underline{x})$  must be approximated. This is accomplished using a Taylor series expansion of  $\underline{h}(\underline{x})$  about the nominal trajectory,  $\hat{\underline{x}}$ :

$$\underline{h}(\underline{x}) = \underline{h}(\hat{\underline{x}}) + \left. \frac{\partial \underline{h}}{\partial \underline{x}} \right|_{\underline{x}=\hat{\underline{x}}} (\underline{x} - \hat{\underline{x}}) + \text{H.O.T.} \quad 3.4$$

$$= \underline{z}_c + \underline{H} \delta \underline{x}, \quad 3.5$$

where:

$\underline{z}_c$  are the predicted values of the observations.

The residuals are expressed as:

$$\underline{r} = (\underline{z}_O - \underline{z}_C) - H\underline{\delta x} . \quad 3.6$$

The weighted least squares criteria is now

$$\frac{\partial}{\partial \underline{\delta x}} (\underline{r}^T \underline{W} \underline{r}) = \frac{\partial}{\partial \underline{\delta x}} ([\underline{z}_O - \underline{z}_C - H\underline{\delta x}]^T \underline{W} [\underline{z}_O - \underline{z}_C - H\underline{\delta x}]) = 0 \quad 3.7$$

where

$\underline{W}$  is the weighting matrix.

The update equations for the state estimate are

$$\underline{\delta x} = (H^T \underline{W} H)^{-1} H^T \underline{W} (\underline{z}_O - \underline{z}_C) \quad 3.8$$

$$\underline{x}_{N+1} = \underline{x}_N + \underline{\delta x} \quad 3.9$$

Because of the nonlinearities in the problem, this process (eqs 3.8-3.9) must be iterated until the solution converges, i.e.  $\underline{\delta x}$  approaches zero.

The matrix  $\underline{W}$  represents the confidence, or expected accuracy, of each observation relative to the other observations. In this study the same weighting matrix is used for all the radar sites providing observations of slant range, azimuth, and elevation. This means that all of the slant range measurements are weighted equally, as well as all of the azimuth measurements and the elevation measurements. The weights used for the slant range, azimuth, and elevation were based on ADCOM D06 Technical Note 79-4 (19) describing

sensor accuracies. The average standard deviation of the error in the range measurements was 47 m or about  $7.4 \times 10^{-6}$  DU (1 DU=6378.145 km). The average standard deviation of the error in the azimuth and elevation measurements was 0.014 deg, or about  $2.4 \times 10^{-4}$  rad. This indicates that a weighting factor for the slant range measurements should be about 1000 times the weighting factor of the azimuth and elevation measurements; however, faster convergence was achieved using a ratio of 100.

The H-matrix is a 3x7 matrix relating changes in the slant range, azimuth, and elevation at the time of the observation to changes in the state at the epoch time,  $t_0$ . These partial derivatives are calculated analytically rather than numerically to reduce the computational load of the filter. H is evaluated using the chain rule, i.e.

$$H = M_1 M_2 M_3 M_4 M_5 \quad 3.10$$

where:

$M_1$  is a 3x3 matrix containing the partial derivatives of slant range, azimuth, and elevation with respect to components of a vector in the THC frame (3).

$$M_1 = \begin{bmatrix} -\cos(Az)\cos(El) & \sin(Az)\cos(El) & \sin(El) \\ \sin(Az)/(\rho\cos(El)) & \cos(Az)/(\rho\cos(El)) & 0 \\ \cos(Az)\sin(El)/\rho & -\sin(Az)\sin(El)/\rho & \cos(El)/\rho \end{bmatrix} \quad 3.11$$

$M_2$  is a 3x3 coordinate transformation from the THC frame to the GEC frame (eq. 2.21)

$M_3$  is another coordinate transformation, this time from the GEC frame to a coordinate frame (UVW) with the  $\hat{u}$  and  $\hat{v}$  basis vectors in the orbital plane and  $\hat{u}$  aligned with the position vector of the satellite.  $M_3$  is given in equation 2.18 with  $u=f+\omega$  replacing  $\omega$ .

$M_4$  is a 3x7 matrix relating changes in the position vector in the UVW frame to changes in the state at some time,  $t$ . Since the UVW frame is not inertial, changes in the direction of the unit vectors must be included. The non-zero elements of  $M_4$  are given below.

$$\begin{aligned}
 M_4(1,1) &= r/a \\
 M_4(1,2) &= (r-a)/e \\
 M_4(1,6) &= a \sin(f) / (1-e^2)^{1/2} - v/n \\
 M_4(2,4) &= r \cos(i) \\
 M_4(2,5) &= r \\
 M_4(2,6) &= a^2 (1-e^2)^{1/2} / r \\
 M_4(3,3) &= r \sin(u) \\
 M_4(3,4) &= -r \sin(i) \cos(u)
 \end{aligned}
 \tag{3.12}$$

$M_5$  is the 7x7 state transition matrix. It is approximately letting

$$\underline{\tilde{x}} = \underline{x}_0 + (t-t_0) \dot{\underline{x}}
 \tag{3.13}$$

and evaluating  $\dot{\underline{x}}$  using values of the state at epoch,  $t_0$ . Only secular and long-period variations in the elements due to drag and the zonal harmonics in the geopotential are included in the calculation of the state transition matrix.

Equation 3.13 is adequate for the variation in the elements due to the geopotential, but does not apply to the variations in the elements due to atmospheric drag due to the presence of position and velocity in the variational equations. King-Hele (8) shows that for small  $(t-t_0)$ , the variations of the elements due to atmospheric drag are governed by:

$$\begin{aligned}
 a &= a_0 - QnBa^2 \rho_p \exp(-z) (I_0(z) + 2eI_1(z)) (t-t_0) \\
 e &= e_0 - QnBa \rho_p \exp(-z) (I_1(z) - e/2(I_0 - I_2)) (t-t_0) \\
 i &= i_0 - 1/4a\omega_e BQ^{1/2} \rho_p \exp(-z) \sin(i) [I_0 - 2eI_1 \\
 &\quad + (I_2 - 2eI_1) \cos(2\omega)] (t-t_0) \\
 \Omega &= \Omega_0 - 1/4a\omega_e BQ^{1/2} \rho_p \exp(-z) [I_0 - 2eI_1] \sin(2\omega) (t-t_0) \\
 \omega &= \omega_0 + 1/4a\omega_e BQ^{1/2} \rho_p \exp(-z) \cos(i) [I_0 - 2eI_1] \\
 &\quad \sin(2\omega) (t-t_0),
 \end{aligned}
 \tag{3.14}$$

where:

$$Q = (1 - r_p \omega_e \cos(i) / v_p),$$

$\rho_p$  is the density at perigee,

$z = ae/H$ , and

the  $I_n$  are the modified Bessel Functions of order  $n$ .

The state transition matrix is given in Appendix B.

The algorithm used to estimate the state using a least squares filter is presented below.

1. Select a batch size,  $m$ , for processing the data.  
Batch sizes of 15 - 25 sets of observations (slant range, azimuth, and elevation) are used in this research.
2. Read in the next  $m$  sets of observations and save as  $\underline{z}_0$ .
3. Propagate the state,  $\underline{x}$ , to each observation time,  $t_i$ , using eq 2.4 and calculate  $\underline{z}_c(t_i)$  and  $H(t_i)$ .  
Combine the  $\underline{z}_c(t_i)$ 's and  $H(t_i)$ 's to form  $\underline{z}_c(t)$  and  $H(t)$ .
4. Calculate  $\underline{\delta x}$  from eq 3.8.
5. Update  $\hat{x}$ , eq. 3.9.
6. Repeat 3 - 5 until solution converges.
7. Propagate  $\hat{x}$ , eq 2.4, to new epoch time (time of last processed observation) and read in next  $m$  data sets.
8. Repeat until all of the data are processed.

### 3.3. Extended Kalman Filter (EKF)

The Kalman filter is a sequential estimator providing an estimate of the state vector based on the system dynamics model and information from all of the previous observations. For a linear problem with Gaussian additive noise the Kalman filter provides an optimal estimate of the state vector. However, for the nonlinear problem, the Kalman Filter no longer guarantees an optimal solution. This is due to the fact that the optimal estimate requires knowledge of the probability density function of the states,  $p(\underline{x}, t)$ . For a nonlinear problem,  $p(\underline{x}, t)$  will not remain a Gaussian density function even though the initial state may be Gaussian and the process noise and observation noise are Gaussian. If  $p(\underline{x}, t)$  is not Gaussian, the estimation of the optimal state vector requires the knowledge of the entire density function, which is not feasible. Therefore, some form of a suboptimal estimator is required. The simplest form is the linearized Kalman filter. The linearized Kalman Filter (16) provides an optimal estimate of the error in the state,  $\underline{\delta x}(t)$ . This error is then added to the nominal state  $\hat{\underline{x}}(t)$  to determine the total state:

$$\underline{x}(t) = \hat{\underline{x}}(t) + \underline{\delta x}(t) \quad 3.15$$

This form of the Kalman filter is adequate if the nominal state is nearly the same as the "true" state; however, if



the nominal state and the "true" state differ by a large amount the linearization is no longer appropriate.

The extended Kalman filter is an attempt to reduce the effect of this problem. The EKF relinearizes about the "new" state after each measurement update. This reduces the difference between the optimal state and the "true" state thus enhancing the assumption that a linearization of the dynamics and observations is valid. The linearized system dynamics and observation equations are obtained by using a Taylor series expansion of the equation about the nominal trajectory. A derivation of the EKF equations is presented by Maybeck (16) and will not be presented here. The resulting EKF equations are (16):

Propagation:

$$\begin{aligned}\dot{\underline{\hat{x}}}(t) &= \underline{f}(\underline{\hat{x}}(t), t), \\ \dot{P}(t) &= F(\underline{\hat{x}}, t)P(t) + P(t)F^T(\underline{\hat{x}}, t) + Q,\end{aligned}\quad 3.16$$

Update:

$$\begin{aligned}K &= P(-)H^T(\underline{\hat{x}}(-)) [H(\underline{\hat{x}}(-))P(-)H^T(\underline{\hat{x}}(-)) + R]^{-1}, \\ \underline{\hat{x}}(+) &= \underline{\hat{x}}(-) + K[\underline{z}_0 - \underline{h}(\underline{\hat{x}}(-))], \text{ and} \\ P(+) &= P(-) - KH(\underline{\hat{x}}(-))P(-),\end{aligned}\quad 3.17$$

where:

$P$  is the state covariance matrix,  
 $F$  is the linearized dynamics matrix,  
 $Q$  is the process noise matrix,  
 $K$  is the filter gain matrix,

H is the linearized observation matrix, and

R is the measurement noise matrix.

The initial values of the state and covariance matrix must be input to the filter. The initial values of the state, called the epoch values, are described in Chapter 4 for each case. The initial value of the covariance is a measure of the confidence in the epoch values of the state. The initial covariance matrix is assumed to be a diagonal matrix with each of the diagonal elements equal to  $1E-06$ . The process noise matrix, Q, is a measure of the uncertainty in the dynamics model. Sources of error in the dynamics include unmodeled forces such as third body perturbations or higher order terms in the geopotential, uncertainties in the modeled geopotential coefficients, and errors in the atmospheric density model. The process noise matrix used in this research is described in Chapter 5. The H-matrix is the same as the H-matrix used in the least squares filter and is described in the previous section. Finally, the measurement noise matrix is a measure of the accuracy of the observations: slant range, azimuth, and elevation. The EKF equations allow the flexibility to use different weights for each type of observation; slant range, azimuth, or elevation, and for each radar site. For the radar sites used in this work, the standard deviations of the measurements did not vary significantly from site to site (19) and

therefore only one measurement noise matrix is used.  $R$  is assumed to be a diagonal matrix. The diagonal elements are equal to the variances in the slant range, azimuth, and elevation measurements respectively. Initial values for the variances were calculated by squaring the average of the standard deviations for each of the radar sites. The average standard deviation of the slant range measurements is 47 m which results in a variance of about  $1E-11 \text{ DU}^2$ . Similarly, the average standard deviations of the azimuth and elevation are 0.14 deg which result in variances of  $5E-08 \text{ rad}^2$ . The values of the elements of the  $R$ -matrix were later altered to improve the filter performance. The values used are reported in the results section, Chapter 5.

Several modifications to the EKF can be incorporated to improve the filter performance. One change is the inclusion of "pseudonoise" (16) in the  $Q$ -matrix and the  $R$ -matrix to compensate for unmodeled errors and errors due to nonlinearities in the problem. This method is used to alter the filter gain and achieve a balance between ignoring the new data (low filter gain) and tracking the noise in the data (high filter gain). Another modification to compensate for nonlinearities in the problem is to add iterations in the propagation and update equations. An iterated, extended Kalman filter which incorporates iterations in the update equations is investigated in this research. The modified update equations are (16):

$$\begin{aligned}
 K(t) &= P(-)H^T(\hat{\underline{x}}(i), t) \\
 &\quad [H(\hat{\underline{x}}(i), t)P(-)H^T(\hat{\underline{x}}(i), t) + R]^{-1} \\
 \hat{\underline{x}}(i+1) &= \hat{\underline{x}}(-) + K(t)\{\underline{z}_O - \underline{z}_C - H(\hat{\underline{x}}(i), t) \\
 &\quad [\hat{\underline{x}}(-) - \hat{\underline{x}}(i)]\},
 \end{aligned}
 \tag{3.18}$$

where:

$P(-)$  is the covariance just before the update,

and

$$\begin{aligned}
 \hat{\underline{x}}(1) &\text{ is the estimate from eq. 3.17,} \\
 &= \hat{\underline{x}}(-) + K[\underline{z}_O - h(\hat{\underline{x}}(-))].
 \end{aligned}$$

Equations 3.18 are iterated until the solution converges or a maximum number of iterations is reached. After the iteration of equations 3.18, the new P-matrix is calculated from equation 3.17.

The algorithm used for the extended Kalman filter is listed below.

1. Read in the initial state vector, covariance matrix, and epoch time.
2. Read in the first data set.
3. Propagate the state vector and covariance matrix to the time of the first observation (eq. 3.16).
4. Calculate the H-matrix and F-matrix.
5. Calculate the gain matrix and update the state vector (eq. 3.17).
6. Repeat 4 and 5 until the solution converges using equation 3.18 to calculate the new gain and the

new state vector.

7. Calculate the updated covariance matrix using equation 3.17.
8. Update the epoch time to the time of the last observation.
9. Read in next data set and repeat steps 3 - 9 until all of the data are processed.

#### 3.4. Second Order Filters

If the nonlinearities in the problem are significant, inclusion of second order terms in the Taylor series expansions of the dynamics and observation equations along with assumptions about the conditional density function of the state based on the observations should improve the filter performance (16). Two filters of this type are developed by Maybeck (16). Only the Gaussian form of the second order filter will be investigated.

As stated before, the optimal estimate of the state,  $\hat{x}(t)$ , based on all of the previous measurements requires the knowledge of the entire conditional probability density function of the state based on the measurements. Since this is not feasible, certain assumptions about the density function must be made. One set of assumptions is to first assume that the density function is symmetric about its mean, thus all of the odd moments of order three and higher are zero. Also, assume that the density function is

concentrated about the mean so that the fourth order and higher order even moments may be neglected. Combining these assumptions with the inclusion of the second order terms in the Taylor series expansions of the dynamics and observation equations results in the truncated second order filter. If the additional assumption that the process noise is time invariant is made, the resulting modified truncated second order filter equations are (16):

Propagation:

$$\begin{aligned}\dot{\hat{\underline{x}}}(t) &= \underline{f}[\hat{\underline{x}}(t), t] + \underline{b}_d(t), \\ \dot{P}(t) &= F[\hat{\underline{x}}(t), t]P(t) + P(t)F^T[\hat{\underline{x}}(t), t] + Q, \quad 3.19\end{aligned}$$

where:

$F$  and  $Q$  are the same as in the EKF, and

$\underline{b}_d(t)$  is an  $n$ -vector whose  $k$ th element is:

$$b_{dk}(t) = (1/2) \text{tr} \left\{ \frac{d^2 f_k}{d\underline{x}^2} \bigg|_{\underline{x}=\hat{\underline{x}}} P(t) \right\};$$

Update:

$$A(t) = H[\hat{\underline{x}}(t-), t]P(t-)H^T[\hat{\underline{x}}(t-), t]$$

$$- \underline{b}_m(t-) \underline{b}_m^T(t-) + R(t),$$

$$K(t) = P(t-)H^T[\hat{\underline{x}}(t-), t]A^{-1}(t),$$

$$\begin{aligned}\hat{\underline{x}}(t+) &= \hat{\underline{x}}(t-) + K(t) [\underline{z}_O - \underline{z}_C - \underline{b}_m(t-)], \text{ and} \\ P(t+) &= P(t-) - K(t) H [\hat{\underline{x}}(t-), t] P(t-),\end{aligned}\quad 3.20$$

where:

H and R are the same as in the EKF, and

$\underline{b}_m(t)$  is an m-vector whose kth element is:

$$b_{mk}(t-) = (1/2) \text{tr} \left\{ \frac{\partial^2 h_k}{\partial \underline{x}^2} \bigg|_{\underline{x}=\hat{\underline{x}}} P(t-) \right\}.$$

Similarly, the Gaussian second order filter is derived by assuming that the conditional probability density function remains Gaussian. The third order and higher order odd moments of a Gaussian density function are zero and the fourth order and higher order even moments can be expressed in terms of the covariance. If only the fourth order moment is considered and the process noise matrix is assumed to be time invariant, the resulting modified Gaussian second order filter equations are the same as the truncated second order filter with the exception of the filter gain,  $A(t)$ , which is now (16):

$$\begin{aligned}A(t) &= H [\hat{\underline{x}}(t-), t] P(t-) H^T [\hat{\underline{x}}(t-), t] \\ &\quad + B(t-) + R(t),\end{aligned}\quad 3.21$$

where:

$B(t-)$  is an m-by-m matrix with klth element:

$$B_{kl}(t-) = (1/2) \text{tr} \left\{ \frac{\partial^2 h_k}{\partial \underline{x}^2} \bigg|_{\underline{x}=\hat{\underline{x}}} P(t-) \frac{\partial^2 h_l}{\partial \underline{x}^2} \bigg|_{\underline{x}=\hat{\underline{x}}} P(t-) \right\}.$$

The differences between the EKF and the second order filters are the additional terms in the dynamics equations, state update equations, and the filter gain. These additional terms in the filter equations can be considered bias terms. These bias terms can be included individually into the filters, making it possible to investigate the effect of each term separately. The dynamics and update bias terms are the same for the two second order filters, so the only difference between the two second order filters is the bias term in the filter gains.

The calculation of the bias terms in the second order filters requires the evaluation of the second partial derivatives of the states at time  $t$ ,  $\underline{x}(t)$ , with respect to the states at time  $t_0$ ,  $\underline{x}(t_0)$ . Since these terms are already second order, only the two-body dynamics plus secular variations due to the Earth's oblateness,  $J_2$ , and atmospheric drag are considered in the bias terms. The derivations of the second order bias terms used in this research are presented in Appendix C.

The algorithm used for the second order filters is the same as the algorithm used for the EKF with the inclusion of the bias terms where appropriate.

The system dynamics and observation equations described in Chapter 2 can now be combined with the filter equations described in this chapter to solve the orbit estimation



problem. The four cases used to compare the performance of the various filters are presented in the next chapter.

## CHAPTER 4

### OBSERVATIONAL DATA

#### 4.1. Introduction

The objective of this research is to compare the performance of several filters using actual satellite tracking data. The first step in the process is to verify the filter algorithms. This is accomplished using synthetic data which is free of process noise and measurement noise. In addition to this test case, observational data obtained from tracking three different satellites are processed in order to compare the performance of the filters. The first satellite orbit is a high altitude (1000 km at perigee), non-circular ( $e=0.015$ ), polar ( $i=90$  deg) orbit. The second orbit is a low altitude (250 km at perigee), non-circular ( $e=0.01$ ), inclined ( $i=72$  deg) orbit. The third satellite orbit is a low altitude (300 km), nearly circular ( $e=0.0003$ ) orbit with an inclination of 50 degrees.

The epoch values for the test case and the three satellite orbits are presented in the next section and a discussion of the data is presented in Section 4.3.

#### 4.2. Epoch Values of the Satellite Orbits

The epoch values for the test case and the three satellite orbits considered in this research are presented

in Tables 4-1 through 4-4. The epoch values for satellites 4507, 6633, and 1 299 are the singularly averaged classical elements provided by the Air Force SPACECOM/DOA. The epoch values for the test case are based on satellite 4507 with small variations in the elements representing initial errors in the state estimate.

Table 4-1

## Epoch Values for the Test Case

Time:	4:24:28.999 on day 19, 1984.
Semi-major axis:	1.1703 DU
Eccentricity:	0.0147
Inclination:	90.076 deg
Longitude of Ascending Node:	293.363 deg
Argument of Perigee:	214.900 deg
Mean Anomaly:	316.080 deg
Ballistic Coefficient:	$0.00698 \text{ m}^2/\text{kg}$

Table 4-2

## Epoch Values for Satellite 4507

Time:	4:24:28.999 on day 19, 1984
Semi-major Axis:	1.1703 DU
Eccentricity:	0.01475
Inclination:	90.077 deg
Longitude of Ascending Node:	293.363 deg
Argument of Perigee:	214.908 deg
Mean Anomaly:	316.078 deg
Ballistic Coefficient:	0.00698 m <sup>2</sup> /kg

Table 4-3

## Epoch Values for Satellite 10299

Time:	23:41:24.000 day 245, 1977
Semi-major Axis:	1.0401 DU
Eccentricity:	0.00955
Inclination:	72.844 deg
Longitude of Ascending Node:	115.989 deg
Argument of Perigee	56.617 deg
Mean Anomaly:	106.653 deg
Ballistic Coefficient:	0.0010 m <sup>2</sup> /kg

Table 4-4  
Epoch Values for Satellite 6633

Time:	22:44:40.000 day 69, 1979
Semi-major Axis:	1.0545 DU
Eccentricity:	0.0003
Inclination:	50.500 deg
Longitude of Ascending Node:	283.827 deg
Argument of Perigee:	169.807 deg
Mean Anomaly:	348.612 deg
Ballistic Coefficient:	0.0120 m <sup>2</sup> /kg

#### 4.3. Data Summary

The observational data used in this research consists of radar passes and observations. A radar pass is the horizon to horizon coverage of a satellite orbit by a particular radar site. An observation is the measured slant range, azimuth, and elevation of a satellite with respect to a particular radar site at a given time. The radar site locations, provided by Air Force SPACECOM/DOA, are given in Appendix D.

The observational data for the test case are synthetic data based on the epoch values of satellite 4507. The data are generated by propagating the initial state forward using the dynamics described in Section 2.2. When the satellite is visible to a radar site a set of look angles; predicted

slant range, azimuth, and elevation, are calculated. For this synthetic data, a radar pass consists of ten sets of look angles, each separated by 60 seconds. These look angles are saved and are used as noise free observational data. There are a total of 100 observations; ten radar passes with ten observations per pass, over a 24 hour period in the test data. This gives one radar pass every 1.35 satellite revolutions. The maximum time between observations is 5.18 hours.

The data for the other three satellites are actual observational data provided by Air Force SPACECOM/DOA. The data include time of observation, satellite number, radar site number, and slant range, azimuth, and elevation of the satellite relative to the site. The radar passes vary from two to 15 observations per pass and the observations in a particular pass are separated by six seconds up to one minute. Also, due to the geometry of the orbits and tasking requirements, radar passes are separated by from a few minutes up to seven hours.

Three days of data, days 19 - 21 in 1984, containing 35 radar passes, are processed for satellite 4507. There are a total of 215 sets of observations, resulting in an average of one radar pass every 1.18 satellite revolutions and an average of 6.1 sets of observations per radar pass. The maximum time between observations is 5.33 hours.

One day of observational data, day 246, 1984, containing 15 radar passes and 72 sets of observations are processed for satellite 10299. This results in an average of one radar pass every 1.07 satellite revolutions and an average of 4.8 sets of observations per radar pass. The maximum time between observations is 4.63 hours.

Finally, the observational data for satellite 6633 consists of 12 radar passes with 68 sets of observations from 22:44 on day 69 through day 70, 1979. This results in an average of one radar pass every 1.37 satellite revolutions with an average of 5.7 observations per radar pass. The maximum time between observations for satellite 6633 is 7.2 hours.

The data are summarized in Table 4-5.

Table 4-5  
Observational Data

Satellite	Hours	Radar Passes	Number of Obs	Revs/ Pass	Obs/ Pass	Maximum Outage (hrs)
Test	24	10	100	1.35	10	5.18
4507	72	35	215	1.18	6.1	5.33
10299	24	15	72	1.07	4.8	4.63
6633	25	12	68	1.37	5.7	7.20

## CHAPTER 5

## RESULTS

5.1. Introduction

The performance of the filters investigated in this research are compared using four criteria. These criteria are estimation errors, prediction errors, computer time of operation, and computer storage requirements.

Estimation errors are based on the state estimate at time  $t(i)$  using all of the observations up to and including time  $t(i)$ . A measure of the filter estimation errors is obtained by comparing the residuals (observed value minus predicted value) in the observations; slant range, azimuth, and elevation, for each filter. Estimation errors are compared in Section 5.2.

Similarly, prediction errors are based on the state estimate at time  $t(i)$  based on observations up to the time  $t(j)$  where  $t(i)$  is greater than  $t(j)$ . Again, a measure of the prediction errors is obtained by comparing the observation residuals of the filters. Prediction errors are compared in Section 5.3.

Finally, computer time of operation and computer storage requirements are discussed in Sections 5.4 and 5.5 respectively.



## 5.2. Estimation Errors

The estimation errors of the filters are compared by comparing the residuals in slant range, azimuth, and elevation for each filter. The filters all start with the same epoch values for each satellite and process three days of data for satellite 4507 and one day of data for the test case (synthetic data based on orbit of satellite 4507), satellite 10299, and satellite 6633. As the data are processed the value of the magnitude of the residuals based on the state estimate after the final iteration are saved and used to calculate the average residuals for each filter. Only the last observation residual from each radar pass is used to calculate the average residual.

The accuracy and stability of the Kalman filter and Gauss filter depend upon the values of the initial covariance matrix, process noise matrix, and measurement noise matrix. If these matrices are not modeled correctly two problems can occur. One possibility is that the estimates of the standard deviations of the state vector, the diagonal elements of the covariance matrix, get very small. This implies that the filter "knows" the state very well and ignores the new data. The true standard deviations of the state vector become much larger than the estimated standard deviations and the filter subsequently diverges. The opposite situation occurs when the estimated standard

deviations of the state are much larger than the true standard deviations of the state. In this case the filter estimate begins tracking the noise in the data and the filter overcompensates for the errors in the state estimate. Values of the initial covariance matrix, process noise matrix, and measurement noise matrix are adjusted by trial and error until satisfactory filter performance is achieved.

The initial value of the covariance matrix is based on the confidence of the initial state vector. The initial state vector is the singularly averaged classical orbital element set provided by SPACECOM/DOA. The state vector in this research consists of the osculating classical orbital elements which differ from the singularly averaged elements by the inclusion of short period variations in the osculating elements. Therefore, the errors in the initial elements are due to differences between these two sets of elements. For example, the magnitude of the short period variation in semi-major axis due to  $J_2$  is about 8 km, or  $1.0E-03$  DU. This results in a standard deviation of  $1.0E-06$  for the semi-major axis. Similar calculations for the other elements provide the remaining diagonal elements for the initial covariance matrix. Starting with these values the diagonal elements of the initial covariance matrix are then varied by trial and error until satisfactory filter performance is achieved. The values for the initial covariance matrix

for the Kalman filter and Gauss filter used for the following comparisons are:

$$P = \text{diag}(1.0\text{E-}06, \dots, 1.0\text{E-}06) \quad 5.1$$

where the units are  $\text{DU}^2$  for the semi-major axis,  $\text{rad}^2$  for the angles, and  $(\text{m}^2/\text{kg})^2$  for ballistic coefficient.

The process noise matrix,  $Q$ , is a function of the unmodeled dynamics and uncertainties in the parameters used in the dynamics model. The initial values of the process noise matrix are based on the values used by Taylor (6). The values are again adjusted by trial and error until satisfactory performance is achieved. The values used in the filters are:

$$Q = \text{diag}(1.0\text{E-}10, 1\text{E-}16, \dots, 1\text{E-}06). \quad 5.2$$

The units for the elements of  $Q$  are  $(\text{DU})^2/\text{TU}$  for the semi-major axis,  $1/\text{TU}$  for eccentricity,  $(\text{rad})^2/\text{TU}$ , for the angles, and  $(\text{m}^2/\text{kg})^2/\text{TU}$  for the ballistic coefficient.

The measurement noise matrix,  $R$ , represents the uncertainty in the observations. Starting values for  $R$  are based on sensor statistics described in Chapter 2. The same matrix is used for all of the radar sites. The measurement noise matrix used here is:

$$R = \text{diag}(1.0\text{E-}10, 1.0\text{E-}07, 1.0\text{E-}07). \quad 5.3$$

The units are  $(\text{DU})^2$ ,  $(\text{rad})^2$ , and  $(\text{rad})^2$ .

The first satellite data investigated in this research is the test case used to verify the filter algorithms which contains no process noise and no measurement noise. The filter estimation errors are presented in Table 5-1.

Table 5-1

## Estimation Residuals of the Test Case

Filter	SR Res (m)	Az Res(deg)	El Res(deg)
LSF	129	0.012	0.0047
EKF	96	0.0028	0.0028
GSF	96	0.0027	0.0029

The errors in Table 5-1 are due in part to the evaluation of the H-matrix and the time between observations. In the formulation of the H-matrix, it was assumed that the orbital elements were nearly constant over the period between the observations so that

$$\underline{x}(t) = \underline{x}(t_0) + \dot{\underline{x}}(t_0)(t-t_0). \quad 5.4$$

This approximation is valid for small  $(t-t_0)$  or if the magnitudes of the variation of the elements,  $\underline{x}(t)$ , are small. However, the average time between observations is a little more than two hours, or 1.35 satellite revolutions. Over this time period, the elements propagate through more than one complete revolution of the short period variations. The magnitude of the short period variations are large

enough to reduce the accuracy of the filters. Since there is no process noise and no measurement noise in the data for the test case, the errors in Table 5-1 are representative of the errors caused by the assumptions made in the use of equation 5-4.

The next satellite investigated in this research is satellite 4507. The orbit of satellite 4507 is nearly polar, has an eccentricity of 0.015, and an altitude of 1000 km. At this altitude atmospheric drag has very little effect on the orbit. The residuals for satellite 4507 are presented in Table 5-2.

Table 5-2

Estimation Residuals for Satellite 4507

Filter	SR Res (m)	Az Res (deg)	El Res (deg)
LSF	140	0.012	0.014
EKF	425	0.070	0.029
GSF	426	0.070	0.028

The residuals in Table 5-2 are based on three days of observations and are the mean of the magnitudes of the last observation residual for each radar pass.

The difference in the magnitude of the residuals between the least squares filter and the recursive filters is due in part to the problem of trying to estimate an unobservable state. At an altitude of 1000 km the atmospheric

density is nearly zero so that the effect of atmospheric drag is insignificant. The orbit of the satellite is independent of the ballistic coefficient so the observations of the orbit provide no information about the ballistic coefficient. This can be checked numerically by checking the condition number of the covariance matrix (20). The condition number of a square, symmetric matrix is a scalar which is the ratio of the maximum eigenvalue to the minimum eigenvalue of the matrix. The magnitude of the condition number is a measure of the numerical stability of the algorithm; the larger the condition number the greater the loss of accuracy in the estimation problem. The condition number of the covariance matrix for the Extended Kalman filter for satellite 4507 is approximately  $1\text{E}+10$ . It is difficult to say much about this case alone, but the condition number for this case can be compared to the condition number for satellite 10299, where the ballistic coefficient should be more observable. The condition number of the covariance matrix for satellite 10299 is  $1\text{E}+06$ .

The condition number itself does not provide information about which state is unobservable; however, for satellite 4507 it is reasonable to assume that the unobservable state is the ballistic coefficient. It is also reasonable to reduce the order of the filter in this case since assuming that the ballistic coefficient is a constant and not

estimating it will not significantly alter the system dynamics; however, it should remove the unobservable state from the problem. The orders of both the Kalman filter and the Gauss filter were reduced by not estimating the ballistic coefficient for satellite 4507. The results of the estimation problem are presented in Table 5-3.

Table 5-3

Estimation Residuals for Satellite 4507  
Using Reduced Order Filters

Filter	SR Res (km)	Az Res (deg)	El Res (deg)
EKF	341	0.069	0.030
GSF	341	0.069	0.030

The condition number for the reduced order Kalman filter covariance matrix is  $1E+07$ .

The next satellite orbit investigated is that of satellite 10299, in a low-altitude ( $h_p = 250$  km), non-circular ( $e = 0.01$ ) orbit, with an inclination of 72 degrees. The estimation residuals for satellite 10299 are shown in Table 5-4.

Table 5-4

Estimation Residuals for Satellite 10299

Filter	SR Res (m)	Az Res (deg)	El Res (deg)
LSF	185	0.048	0.035
EKF	221	0.059	0.057
GSF	189	0.052	0.041

The condition number for satellite 10299 is  $1E+06$ .

The improvement of the Gauss filter over the Kalman filter can be further investigated by considering each bias term individually. The bias terms in the Gauss filter have been described in Chapter 3. There are bias terms in the dynamics, observations, and filter gain. The data for satellite 10299 is processed using the Gauss filter, first with no bias terms, then with only the dynamic bias term, the observation bias term, and the gain bias term individually. The results are presented in Table 5-5.

Table 5-5

Effect of Bias Terms in the Gauss Filter  
for Satellite 10299

Bias Term	SR Res (m)	Az Res (deg)	El Res (deg)
None	221	0.059	0.057
Dynamics	221	0.059	0.057
Observations	189	0.052	0.041
Gain	220	0.059	0.057
All	189	0.052	0.041

The results indicate that the bias term in the observation equations provides the most significant improvement for the Gauss filter. It is also noted that the Gauss filter with no bias terms reduces to the Kalman filter.

The final satellite case considered is satellite 6633, which is in a nearly circular ( $e=0.0003$ ), low altitude



(h=300 km) orbit with an inclination of 50 degrees. Satellite 6633 is known to be Skylab which is non-symmetric and tumbling; therefore, the ballistic coefficient is not constant. The estimation residuals for satellite 6633 are presented in Table 5-6.

Table 5-6

## Estimation Residuals for Satellite 6633

Filter	SR Res (m)	Az Res (deg)	El Res (deg)
LSF	106	0.028	0.013
EKF	512	0.098	0.151
GSF	474	0.090	0.150

As was done for satellite 10299, the bias terms for the Gauss filter can be investigated individually for satellite 6633. The results are presented in Table 5-7.

Table 5-7

Effect of Bias Terms in the Gauss Filter  
for Satellite 6633

Bias Term	SR Res (m)	Az Res (deg)	El Res (deg)
None	512	0.098	0.151
Dynamics	512	0.098	0.151
Observations	614	0.117	0.140
Gain	485	0.093	0.151
All	474	0.090	0.150

The condition number for the Kalman filter covariance matrix for satellite 6633 is  $1E+08$  which is about 100 times larger than the condition number for satellite 10299. This indicates that there may be an unobservable state for this case also. An attempt was made to process the data using the reduced order filter described previously (where all elements but ballistic coefficient are estimated); but the filter eventually diverged and did not yield meaningful results. Prior to the filter divergence the condition number was the same as before,  $1E+08$ , indicating that the unobservable state(s) is not ballistic coefficient. This is reasonable since for a circular orbit the argument of perigee and mean anomaly are undefined. The condition number does not identify the unobservable state(s); however, the physical situation indicates that the argument of perigee and mean anomaly are unobservable for satellite 6633.

The large condition number can be used to explain the large residuals for the recursive filters. A large condition number indicates numerical instability and the recursive filters are inherently less robust than the least squares filter. This is further supported by the increase in the residuals when only the observation bias term is included in the Gauss filter. Normally, the inclusion of second order terms in the filter should improve the filter performance, or at worst, not change the filter performance.

In this case, including the observation bias term, the additional term in the filter equations caused the filter to diverge, resulting in larger residuals.

### 5.3. Prediction Errors

The filter prediction errors are those errors which result from propagating the filter states forward in time without updating the state vector estimate using the observations. The prediction errors are based on the state estimate at time  $t(i)$  based on observations up to time  $t(j)$ , where  $t(j)$  is less than  $t(i)$ . The state vector estimates used in this section to determine the prediction errors are the final values of the state vectors used in Section 5.2. The state vector estimate at time  $t(j)$  is the state vector at the time of the last observation processed in the estimation problem. This estimate is then propagated forward using the full equations of motion described in Chapter 2. The prediction errors are calculated by comparing the predicted value of the observations with actual radar observations of the various satellites.

$$\underline{r} = \underline{z}_o - \underline{z}_c \quad 5.5$$

The vector of residuals is made up of residuals in slant range, azimuth, and elevation.

Figures 5-1 to 5-3 show the prediction errors for satellite 4507 ( $h=1000\text{km}$ ,  $e=0.015$ ,  $i=90^\circ$ ). The epoch

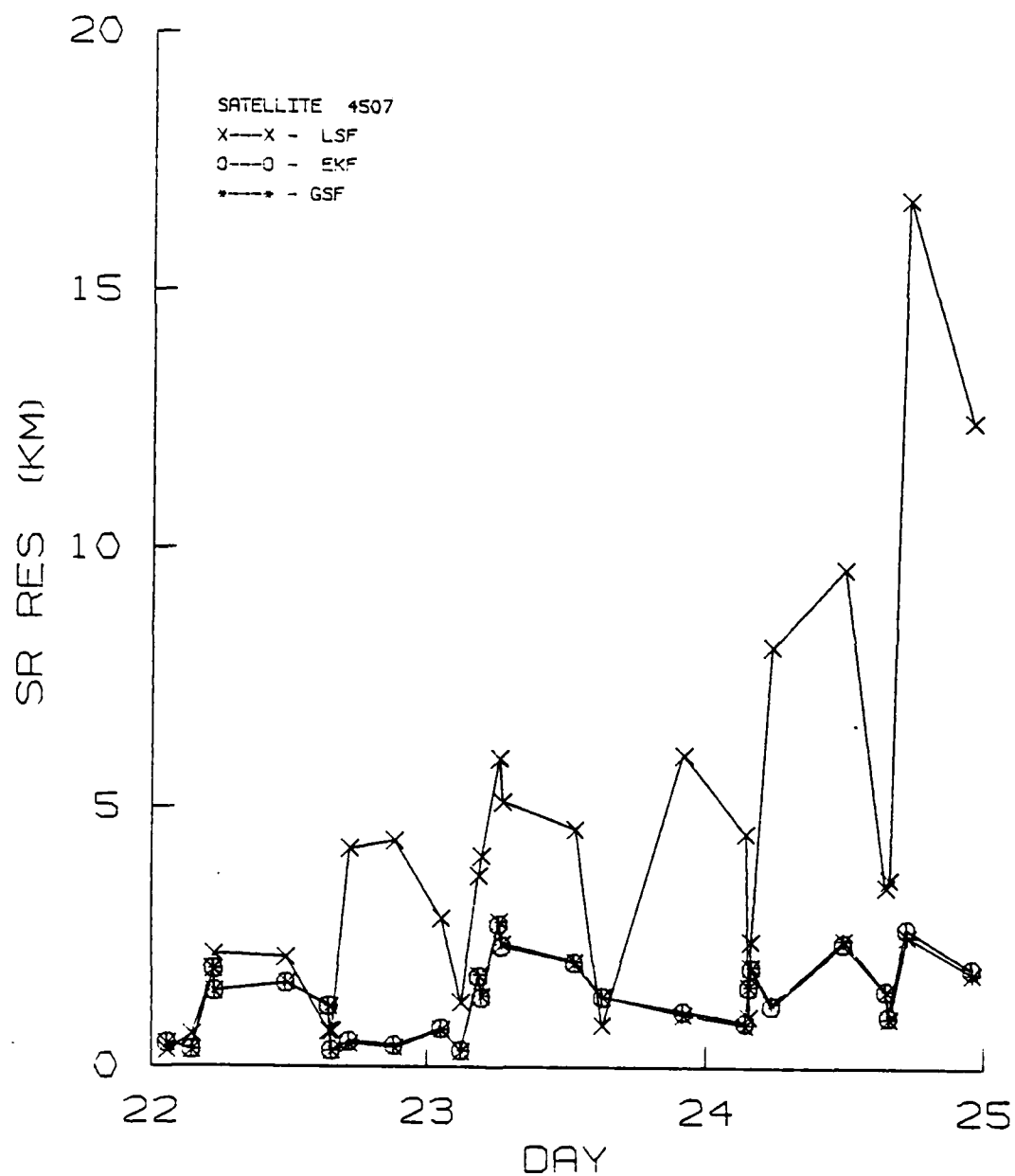


Figure 5-1. Slant Range Prediction Errors for Satellite 4507

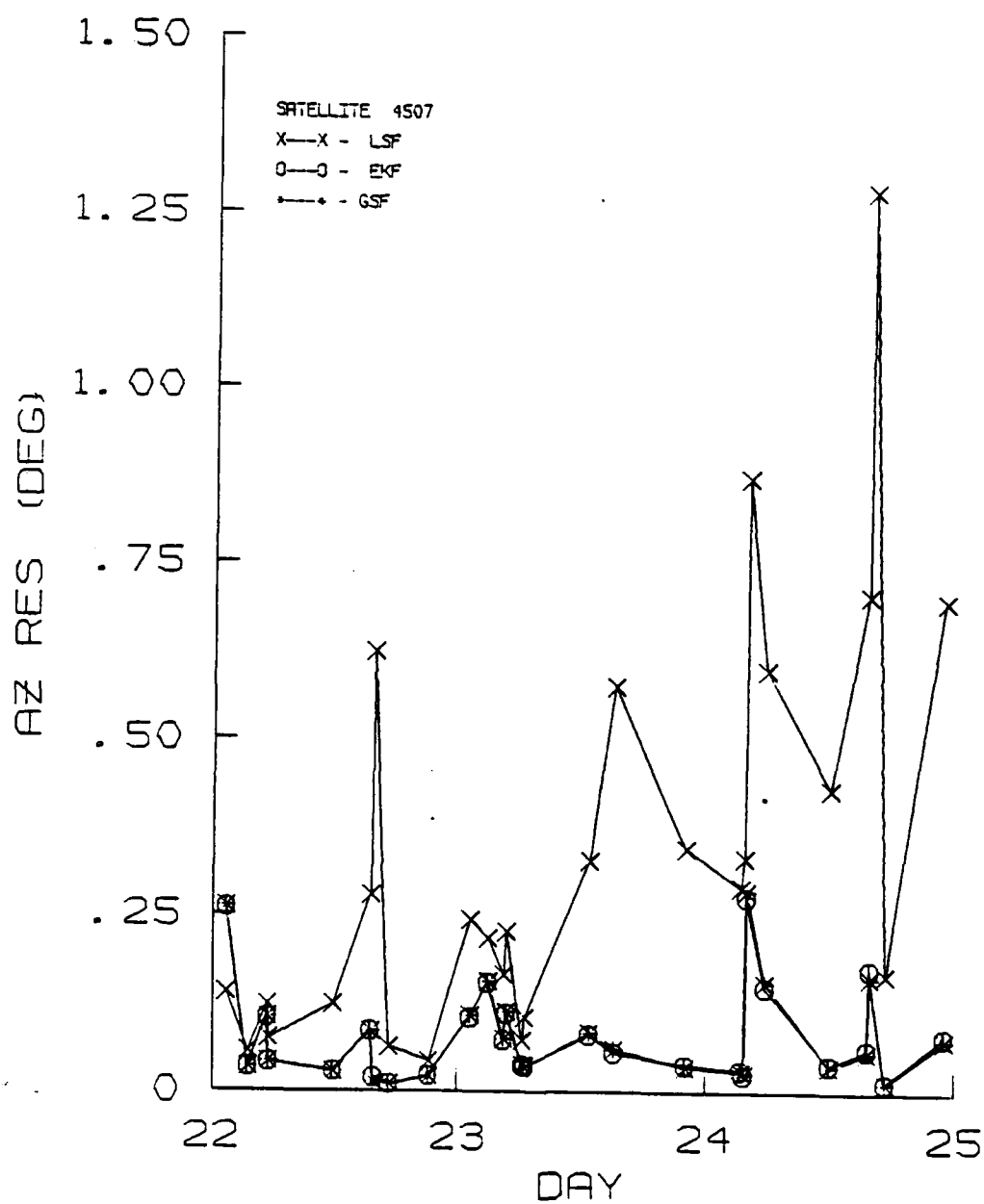


Figure 5-2. Azimuth Prediction Errors for Satellite 4507

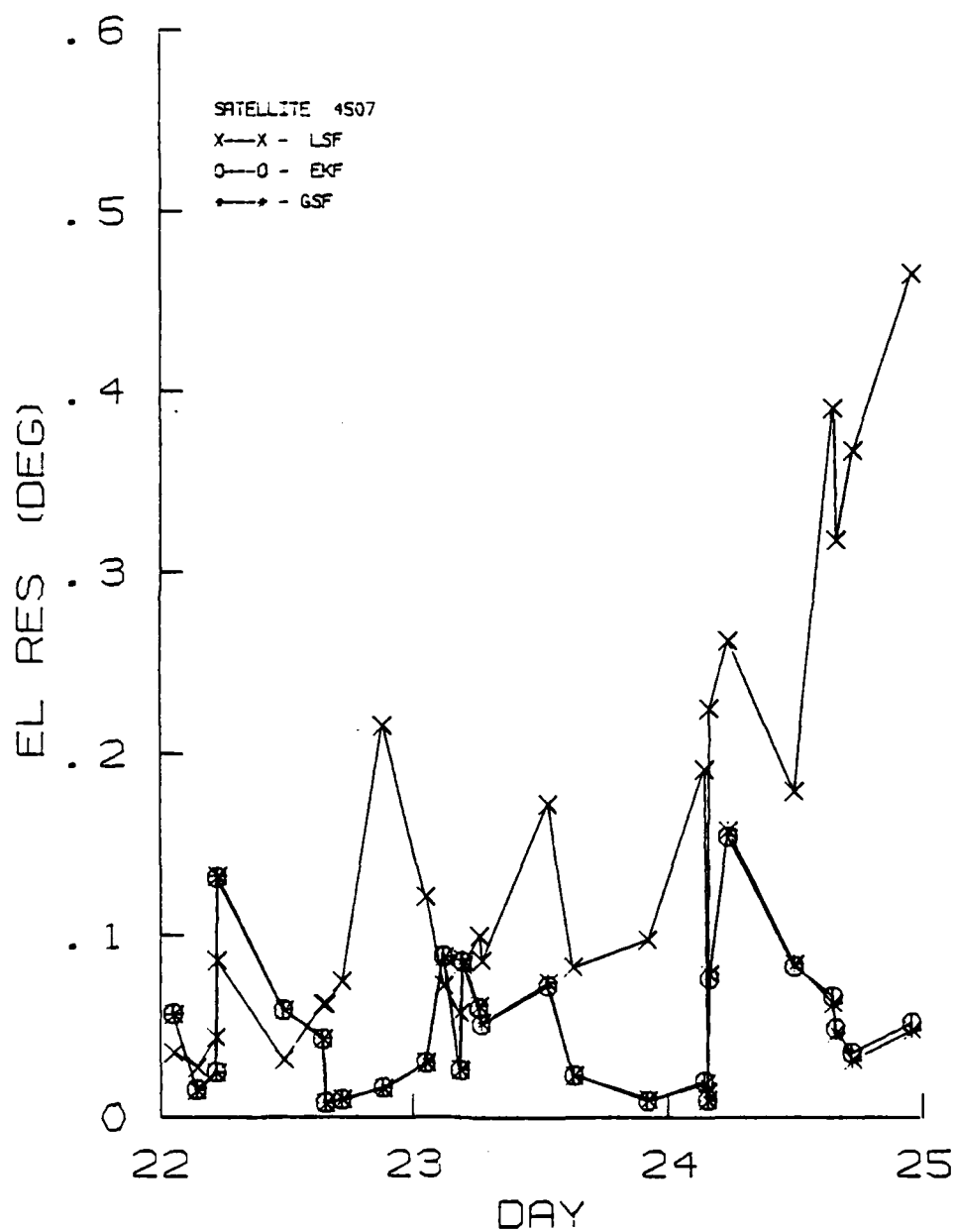


Figure 5-3. Elevation Prediction Errors for Satellite 4507

values of the state vector estimate are the final values of the state vector after processing three days of observational data using the full order filters; the filters estimate the classical orbital elements plus ballistic coefficient. The prediction errors are evaluated for three days following the last measurement update. The points shown in the figures are the average residual for the previous ten observations.

Figures 5-4 to 5-6 are again prediction errors for satellite 4507. These plots are based on the state vector estimate from the reduced order filters; ballistic coefficient is not estimated. For both sets of filters the prediction errors for the two recursive filters, the Extended Kalman filter and the Gauss Filter, are nearly identical to satellite 4507. Also, there is little difference in the prediction errors between the original filters and the reduced order filters. Finally, the prediction errors for the recursive filters appear to be steady while the least squares filter errors appear to be growing linearly. This linear growth in the prediction errors is due to an error in the estimate of the semi-major axis at the beginning of the prediction span. This initial error in the semi-major axis results in a timing error in the prediction of the position of the satellite. In other words, the predicted position of the satellite may be very accurate,

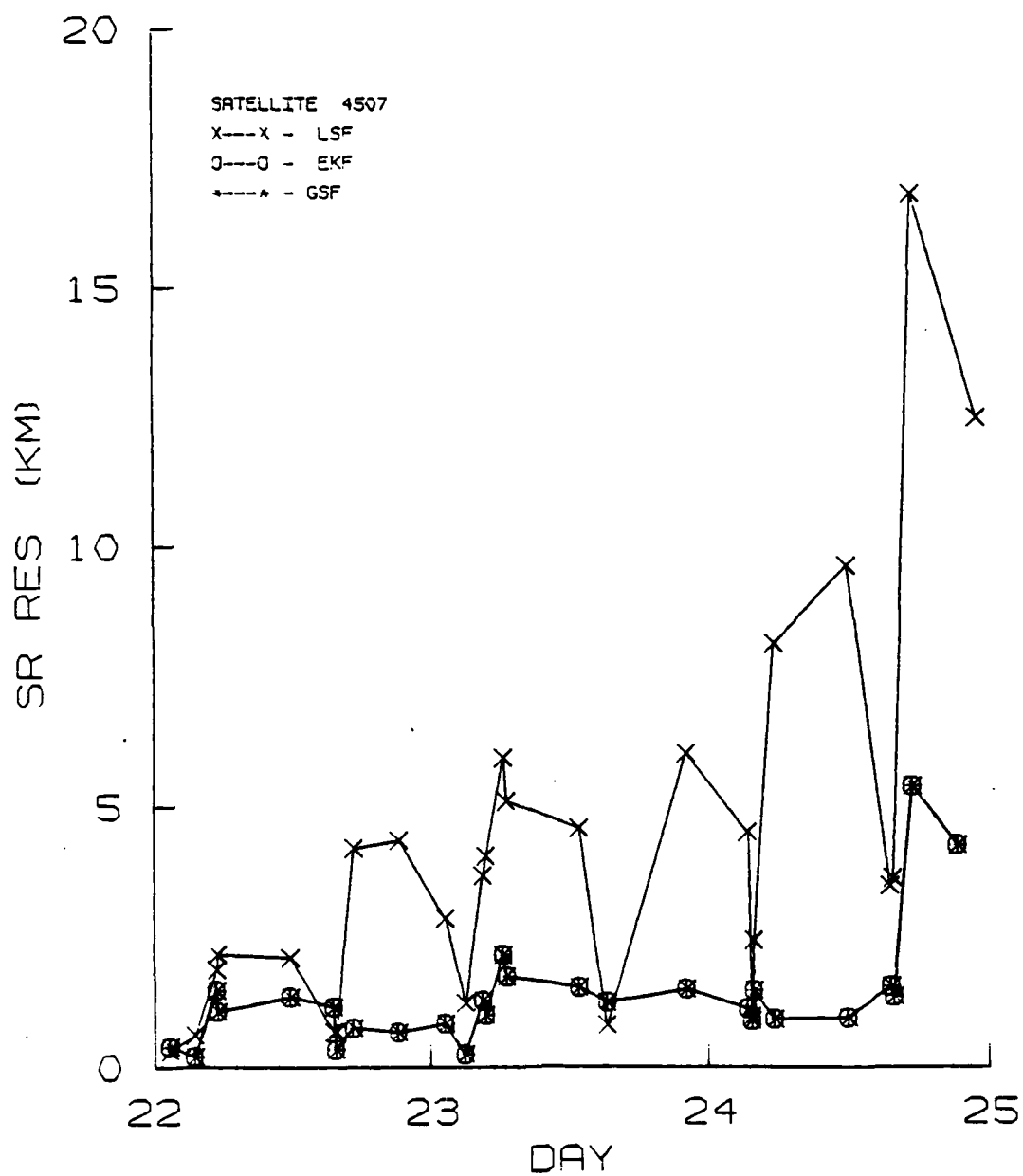


Figure 5-4. Slant Range Prediction Errors Using Reduced Order Filters



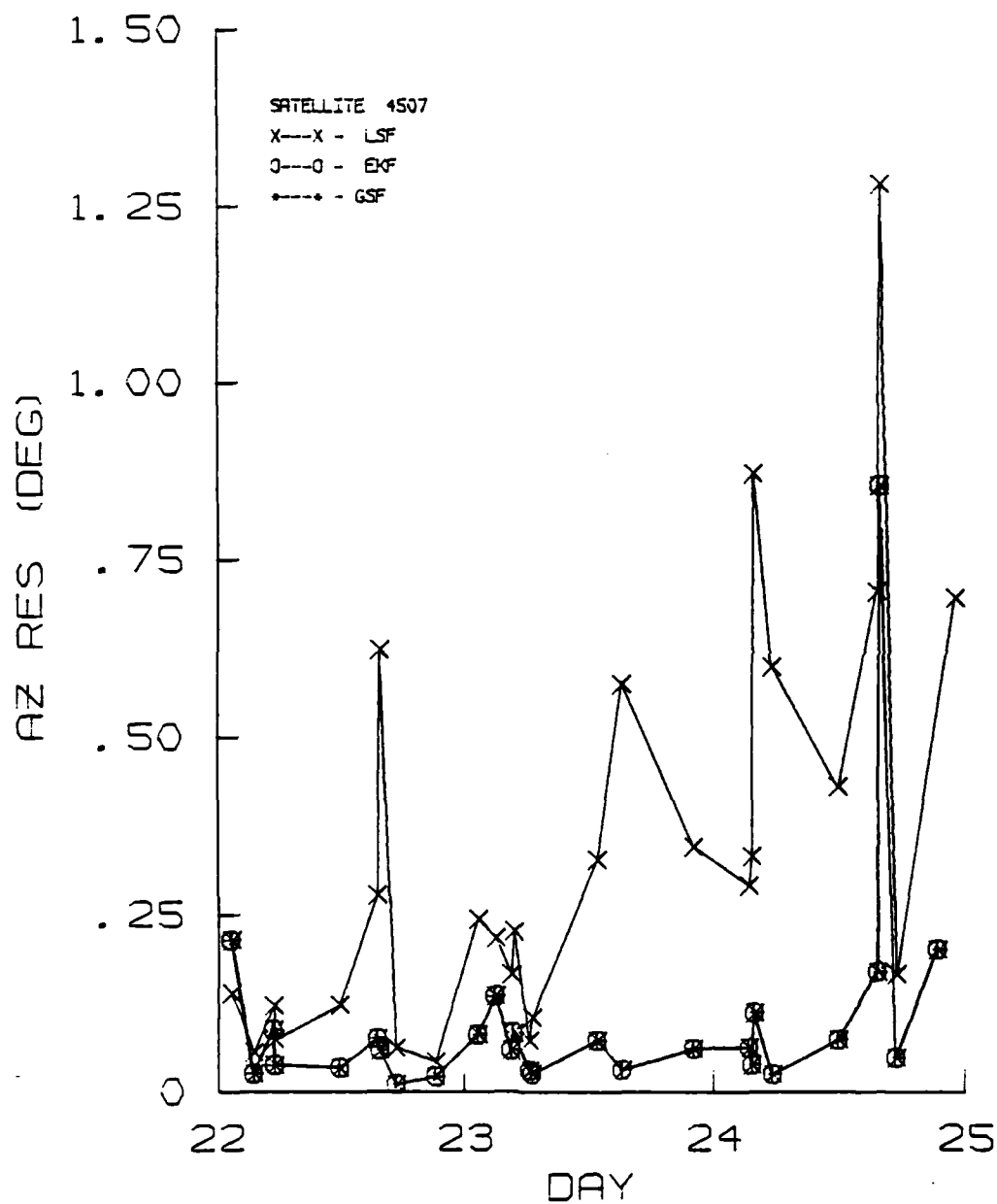


Figure 5-5. Azimuth Prediction Errors Using Reduced Order Filters

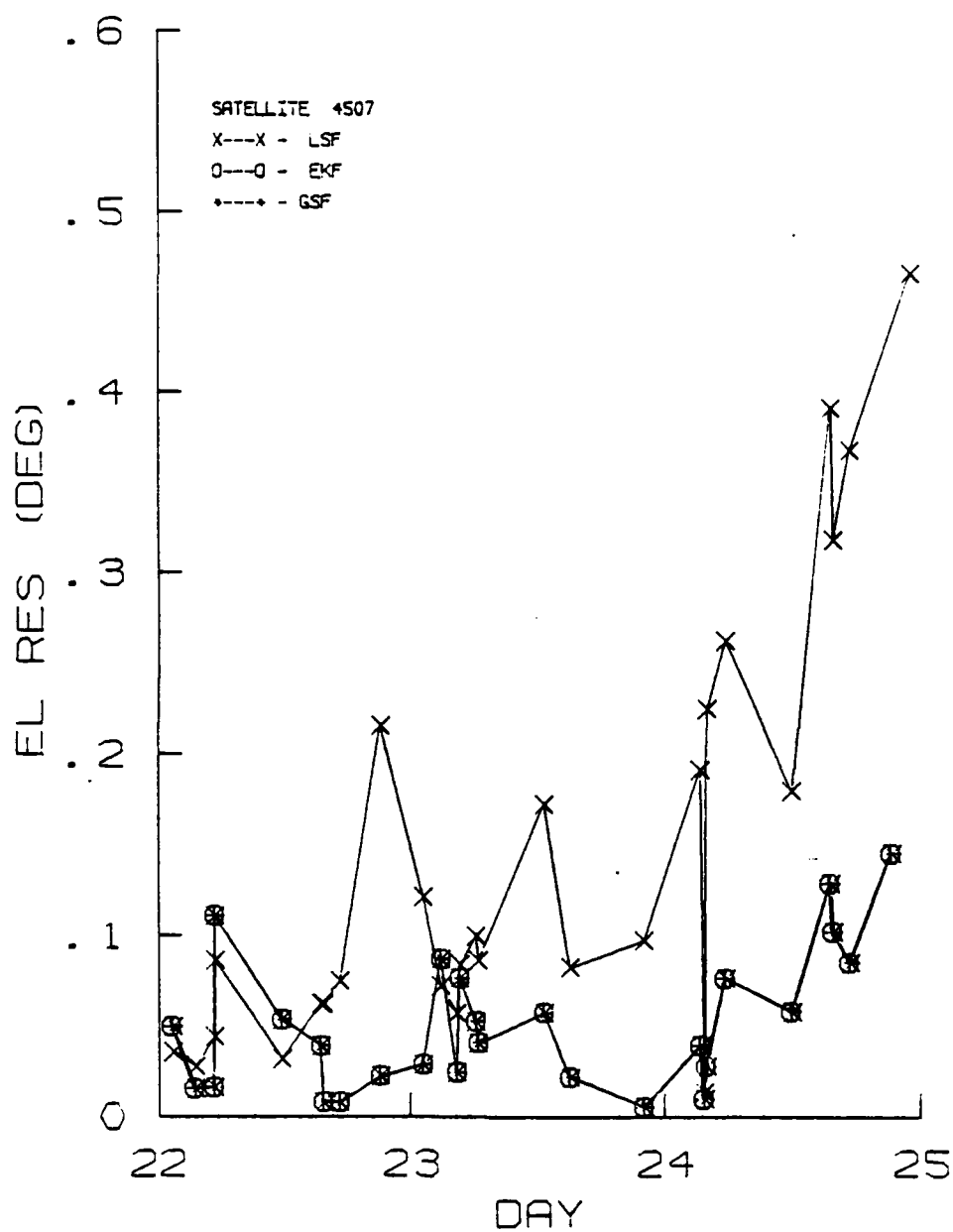


Figure 5-6. Elevation Prediction Errors Using Reduced Order Filters

but the satellite arrives either earlier or later than the predicted time. At the time of the observation for which the residuals are calculated the predicted position of the satellite is calculated for a different point in the orbit. The position of the satellite in the orbit, the true anomaly of the satellite, is calculated by integrating the mean motion of the satellite which is a function of the semi-major axis. Therefore, errors in the semi-major axis are integrated forward with time, resulting in a linear growth in the predicted true anomaly of the satellite. This linear growth in the residuals is apparent in the plots of residuals for the least squares filter.

An important observation can be made from comparing the estimation errors with the prediction errors for satellite 4507. Even though the estimation errors for the least squares filter are smaller than the estimation errors for both the Kalman and Gauss filters, the prediction errors for the Kalman and Gauss filters start out nearly the same as the least squares filter and remain small while the prediction errors for the least square filters have a linear growth. This indicates that even though the least squares filter is fitting the data better (smaller estimation residuals), the Kalman and Gauss filters have a better estimate of the true state vector (smaller prediction residuals). The estimation residuals are obtained by

only fitting the position data (range, azimuth, and elevation) from the radar observations. The propagation of the orbit forward in time without measurement update requires a knowledge of the velocity as well as the position of the satellite. Therefore, the least squares filter appears to be providing a better estimate of the position of the satellite, and the Kalman and Gauss filters appear to be providing poorer estimates of the position but better estimates of the velocity of the satellite.

Similar results were obtained for the prediction errors for satellite 4507 when the state estimates from the filters at different times were used to generate the prediction residuals.

The prediction residuals for satellite 10299 ( $h = 250\text{km}$ ,  $e=0.01$ ,  $i=72^\circ$ ) are shown in Figures 5-7 to 5-9. The filter state vector estimates are propagated forward one day. The points on the plots represent the average of the five previous residuals. The state estimate for the Gauss filter is the state estimate using all three biases; dynamics, observations, and gain, in the filter equations. The linear growth in the residuals is present for the least squares filter and the Kalman Filter for this satellite; however, the residuals for the Gauss filter are nearly constant. Since the orbit of the satellite is affected by drag the growth in the residuals due to a timing error also

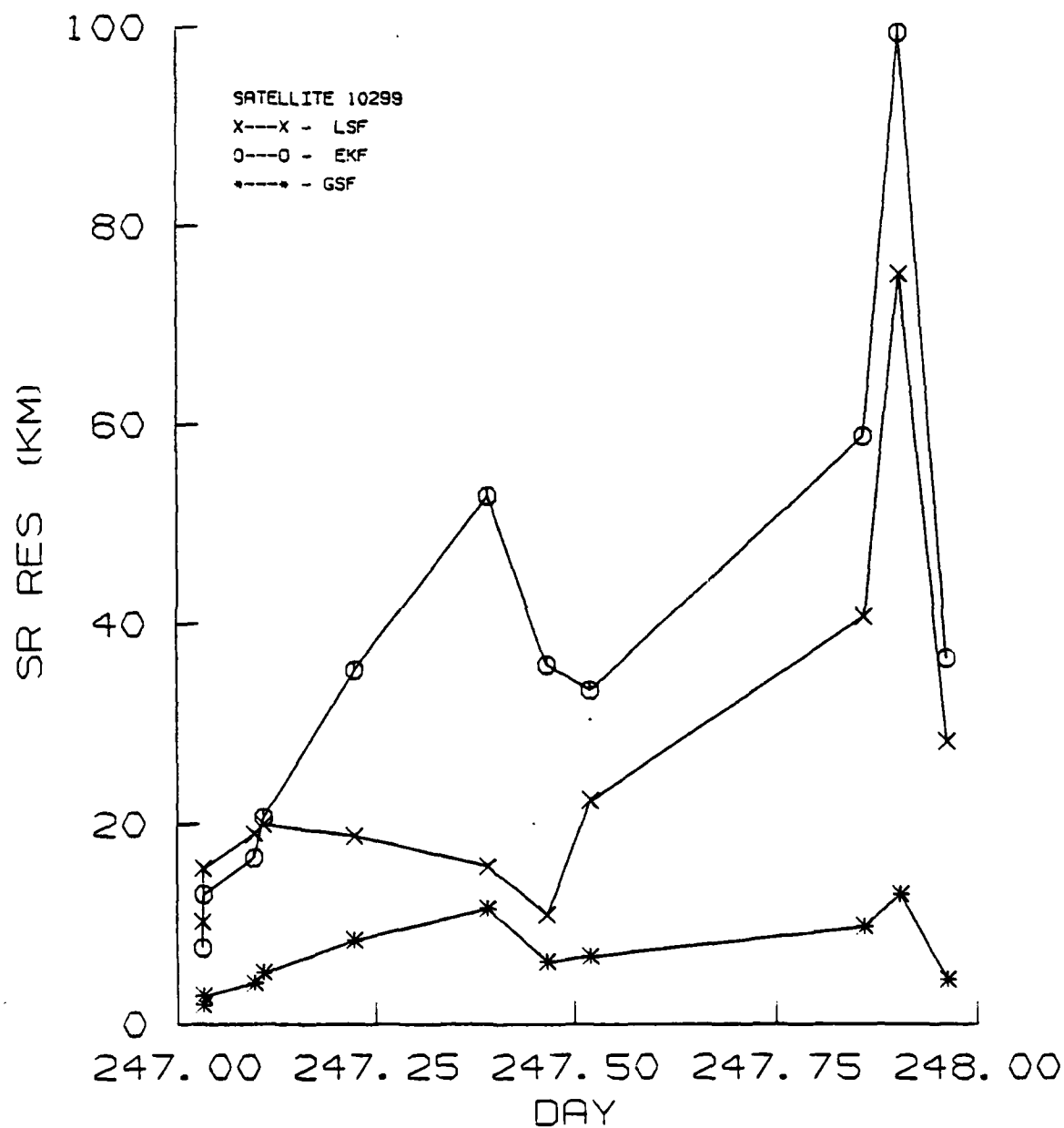


Figure 5-7. Slant Range Prediction Errors for Satellite 10299

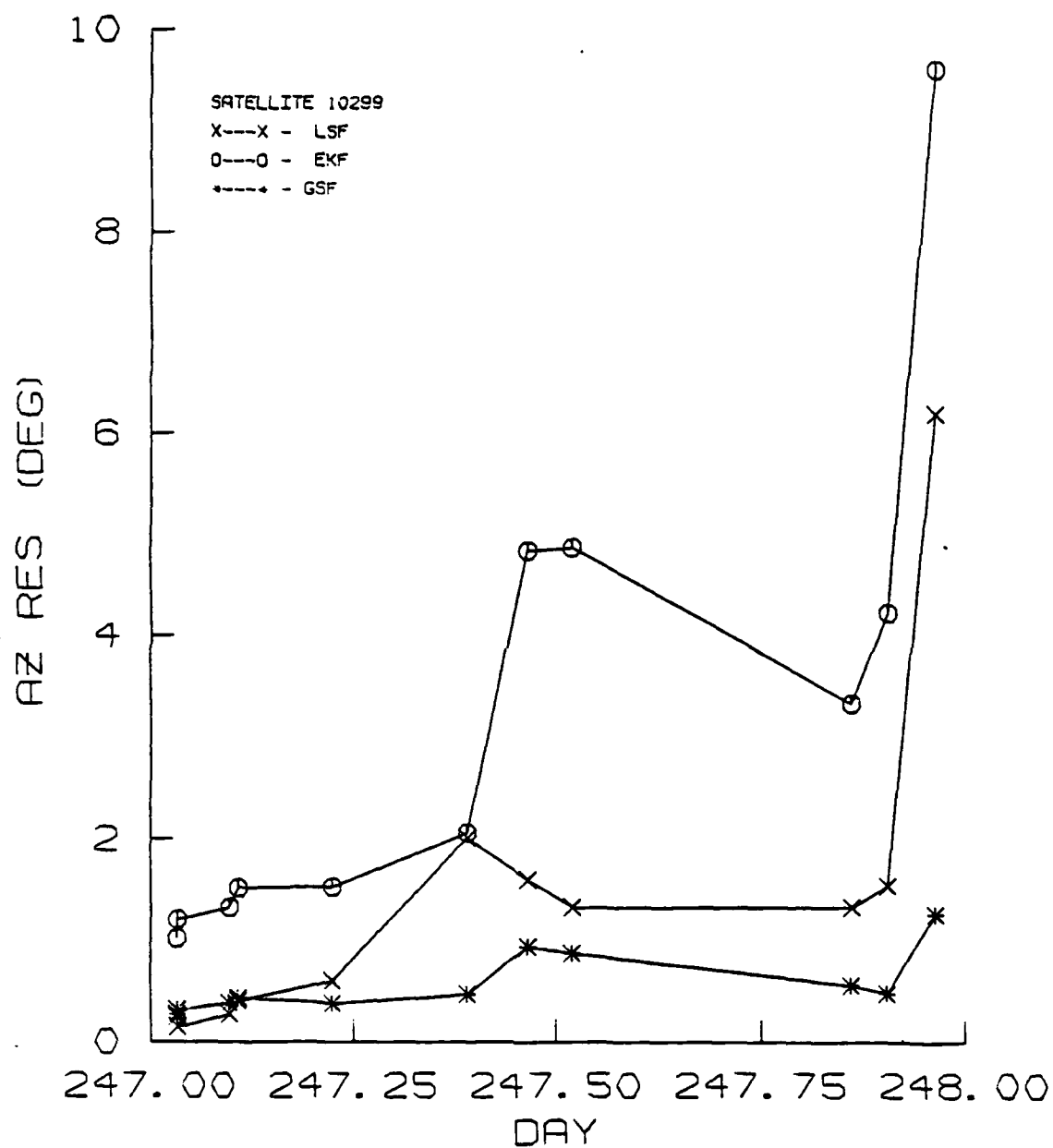


Figure 5-8. Azimuth Prediction Errors for Satellite 10299

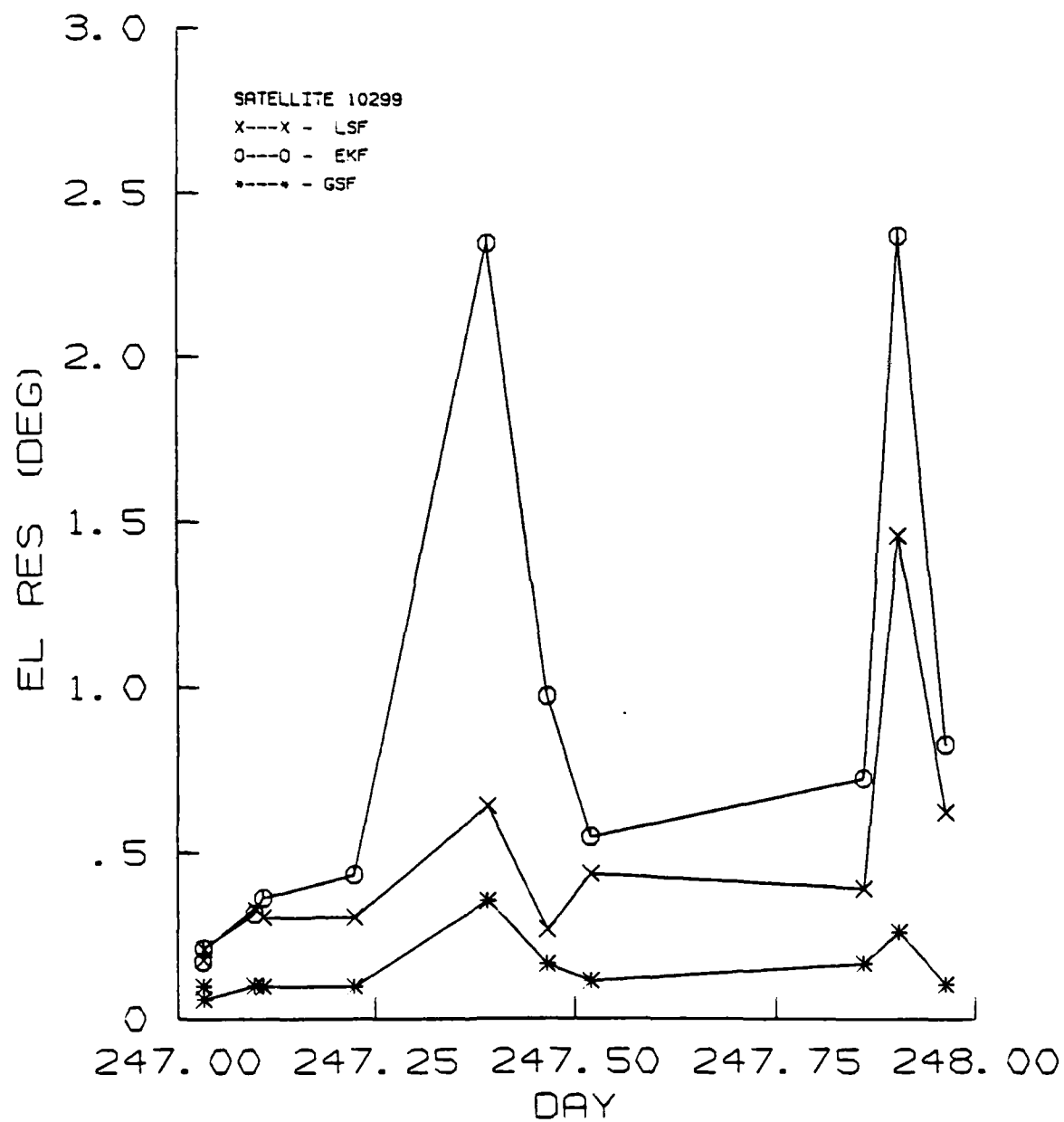


Figure 5-9. Elevation Prediction Errors for Satellite 10299

has a quadratic term. In addition to the integration of the initial errors in the semi-major axis, errors in the semi-major axis and ballistic coefficient result in errors in the magnitude of the drag perturbation. These errors are integrated once to obtain the semi-major axis and once again to obtain the true anomaly, resulting in a quadratic growth in the timing error and therefore in the prediction residuals.

Figures 5-7 through 5-9 clearly show the advantage of including the second order terms in the filter equations. The predicted orbit based on the state vector estimate from the Gauss filter provides a much better match to the observed orbit (position and velocity) than the estimate from either the least squares filter or the Kalman filter.

Figures 5-10 through 5-12 are the prediction residuals for satellite 6633 ( $h=300\text{km}$ ,  $e=0.0003$ ,  $i=50\text{ deg}$ ). The state estimates are propagated forward for two days and the points on the curves represent the average of the previous five residuals. Again, the state vector estimate for the Gauss filter is based on the estimate using all three bias terms in the filter equations. Significant growth in the residuals appears in the plots for the Kalman and Gauss filters; however, the prediction errors for the least squares filter are nearly constant. The initial errors for the Kalman and Gauss filters are also much larger than for the previous cases. The large initial residuals in the



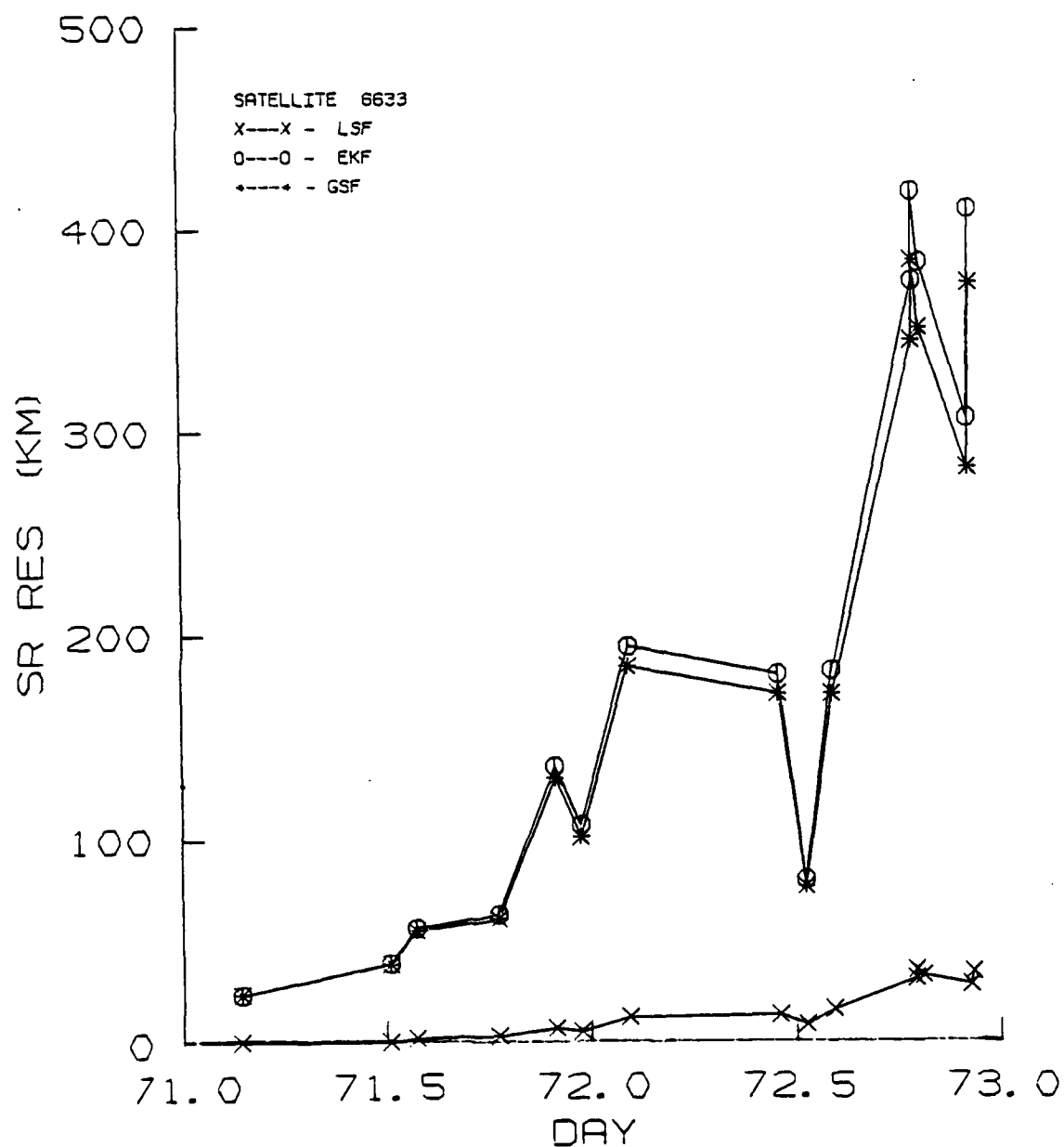


Figure 5-10. Slant Range Prediction Errors for Satellite 6633

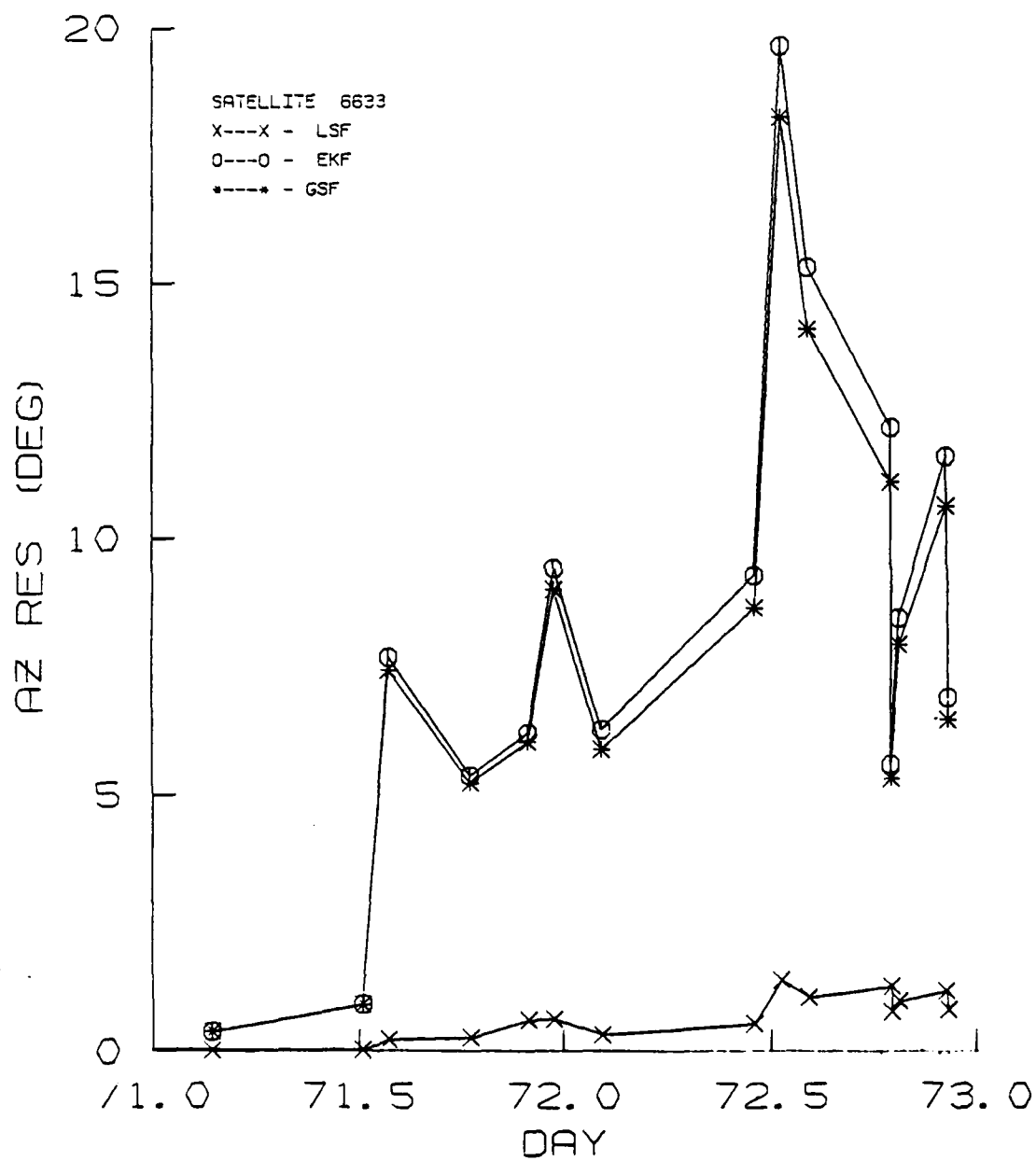


Figure 5-11. Azimuth Prediction Errors for Satellite 6633

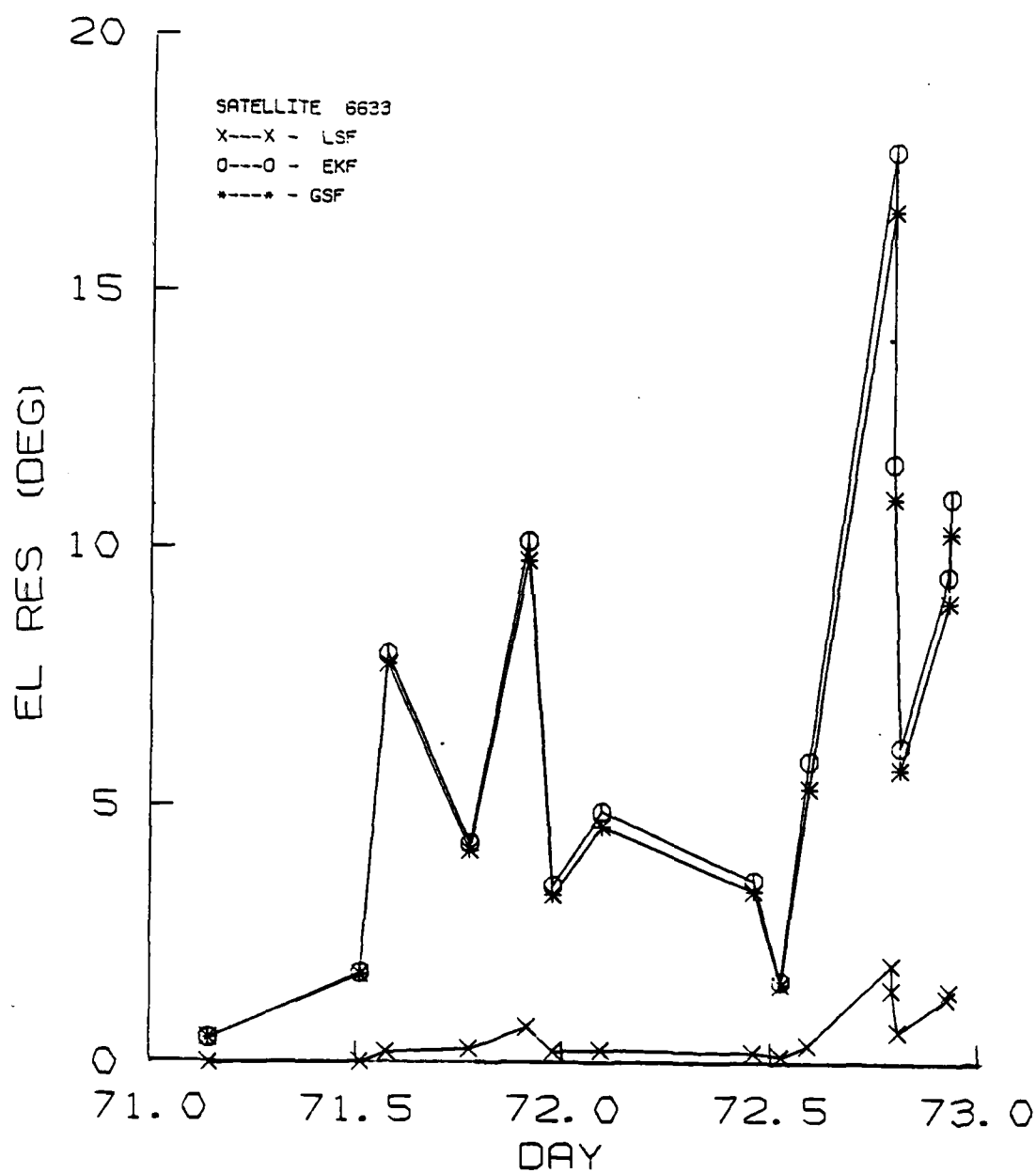


Figure 5-12. Elevation Prediction Errors for Satellite 6633

propagated states are indicative of large errors in the state vector estimate at the end of the estimation sequence. This result is not unexpected since the condition number for the covariance matrix for satellite 6633 is 100 times larger than that for satellite 10299. This large condition number indicates one or more unobservable states. Loss of numerical accuracy and instability can be expected when the condition number is large. Physically this is reasonable because the orbit for satellite 6633 is nearly circular making it very difficult to determine argument of perigee and mean anomaly. In spite of these numerical problems, the estimate from the least squares filter does not diverge and provides an adequate estimate of the orbit of the satellite for re-acquisition based on the predicted look angles.

#### 5.4. Computer Time of Operation

The computer time of operation is the computer execution time required to process the data used in Section 5.2 to determine the estimation residuals. The data are described in Chapter 4. The time of operation for the Gauss filter is presented for several different cases. GSF(D) is the Gauss filter with the dynamic bias only, GSF(O) is the Gauss filter with only the observation bias, GSF(G) is the Gauss filter with the gain bias only, and

GSF(A) is the Gauss filter with all of the bias terms included.

The computer times for the filters for each satellite case are shown in Table 5-8.

Table 5-8

Computer Time of Operation (sec)

Filter	Satellite			
	Test Case	4507	10299	6633
LSF	89.3	125.3	98.2	216.1
EFK	18.1	39.0	19.5	29.6
GSF(D)	-	-	32.9	55.7
GSF(O)	-	-	25.8	36.4
GSF(G)	-	-	26.0	36.7
GSF(A)	32.1	77.4	38.8	59.6

The Air Force Space Command is responsible for maintaining current orbital element sets for about 6000 objects orbiting the Earth. Of the objects, 300 - 350 are active satellites and the remainder are debris. The reduction in the amount of computer time required for the problem of element set maintenance for the satellites listed in Table 5-8 becomes even more significant when applied to a large number of satellites.

### 5.5. Computer Storage Requirements

The computer storage requirements for the three filters are compared in this section. The data shown in Table 5-9 are the computer memory required to load and run the object codes and supporting software for each of the filters. There is not a significant difference; however, the data do not include the memory required for storing data prior to batch processing for the least squares filter. This amount of storage can become significant for element set maintenance for a large number of satellites.

Table 5-9

Computer Storage Requirements (k of memory)

Filter	Storage (k)
LSF	126.0
EKF	120.1
GSF	123.0

## CHAPTER 6

## CONCLUSIONS AND RECOMMENDATIONS FOR FUTURE WORK

6.1. Conclusions

Several conclusions can be drawn from the results presented in Chapter 5.

1. The state vector estimate from the Gauss filter provides the best estimate for propagating the state vector forward in time for satellites 4507 and 10299. The prediction residuals for satellite 10299 clearly show that the smallest residuals result from the propagation of the GSF state vector. The orbit of satellite 10299 ( $h=250\text{km}$ ) is typical of a large number of satellites currently in orbit around the Earth. These orbits are non-circular and have low altitudes where the perturbations due to the non-spherical Earth and to atmospheric drag are most significant. For satellite 4507 the prediction residuals for the EKF and GSF are nearly identical and smaller than the LSF residuals. The nearly identical results from the Kalman and Gauss filters for satellite 4507 are not unexpected. The orbit of satellite 4507 is at a high altitude ( $h=1000\text{km}$ ) where the perturbations due to a non-spherical Earth and atmospheric drag are nearly zero; therefore, the second order terms in the Taylor series should have little effect on the problem of orbit determination. The estimates from

the Kalman and Gauss filters for satellite 6633 diverged due to singularities in the orbit determination problem for this orbit ( $e=0.0003$ ); however, the least squares filter provided an adequate estimate of the state vector for predicting the future position and velocity of the satellite.

2. The least squares filter estimate of the state vector results in the smallest estimation residuals when processing data for all three satellites. The largest difference in estimation residuals is for satellite 6633 which is in a nearly circular orbit. The problem of determining the classical orbital elements of a circular satellite is singular. For nearly circular orbits, the Kalman and Gauss filters experience numerical problems and the estimates diverge. The LSF appears to be more robust and less susceptible to numerical problems.

3. The Gauss filter estimation residuals are equal to or smaller than the estimation residuals for the Kalman Filter. The biggest improvement is for satellite 10299. The orbit of satellite 10299 is low altitude ( $h=250$  km) and noncircular ( $e=0.01$ ) representing a case where the determination of the classical orbital elements is non-singular. In addition, the perturbing accelerations due to atmospheric drag and the non-spherical Earth are significant. Little or no improvement in the estimation residuals for the Gauss filter is observed for satellite 4507 where the



perturbing accelerations are nearly zero. This is in agreement with the conclusions of Tapley and Choe (5) and Athens et al. (7). They both report that the second order filters provide the greatest improvement over the Kalman filter when the perturbations are the most significant. Little can be concluded from the results for satellite 6633 due to the singularities in the problem.

4. The Extended Kalman filter is much faster than the least squares filter and the Gauss filter. The EKF is about twice as fast as the GSF in processing the data for all three satellites and nearly five times as fast as the LSF. The GSF processes the data two to three times faster than the LSF. These differences in process time become even more significant when applied to the problem of maintaining current orbital element sets for 6000 satellites.

5. The computer storage requirements are nearly the same for all three filters. The computer storage requirements do not address the need to store the observations of the satellites prior to batch processing by the least squares filter.

6. The most significant second order terms in the filter equations are found in the observation equations. The inclusion of the bias terms for the dynamics and gain in the filter equations result in no measurable improvement

in the Gauss filter performance. Taylor (6) also reported that greatest effect due to the nonlinearities in the orbit determination problem are caused by nonlinearities in the observation equations. This is in contrast to the work of Tapley and Choe (5), who reported that the most significant bias term in the interplanetary problem is the gain bias term while Athans, et al. (7) reported that the dynamic bias term was the most significant bias term for a vertically falling body. This problem can be explained by the fact that these two estimation problems are qualitatively quite different from the determination of the orbit of an Earth satellite.

The inclusion of the bias term for the observations in the filter improves the Gauss filter performance for satellite 10299, but results in no change for satellite 4507. Little can be concluded for satellite 6633 due to the singularity in the problem of determining the classical orbital elements for a nearly circular orbit.

7. The reduced order filters (in which ballistic coefficient was removed from the estimation state vector) for the high altitude satellite 4507 reduce the estimation residuals for the Kalman and Gauss filters.

## 6.2. Recommendations for Future Work

1. The orbit determination problem for satellite 6633 presents several problems due to the singularities

in the classical orbital elements. Also, estimating the osculating elements results in large short period variations in the state vector over relatively short time periods. This presents two problems. First, the step size for the numerical integrator is a function of the magnitude of the variations of the state vector. Also, the assumptions made in equation 3.13 to calculate the state transition matrix introduces errors into the problem when the elements of the state vector are not constant over the period of interest. A transformation of variables from the state vector used in this research to a set of mean, non-singular elements should improve the filter performance. One set of elements well suited to the orbit determination problem is the set of mean equinoctial elements (3). The equations of motion and observation equations described in Chapter 2 should be converted to the mean, equinoctial set of orbital elements and the filter comparisons described in Chapter 5 should be repeated.

2. A large portion of the computer operation time is required to propagate the state vector from one observation to the next. This method of special perturbations is accurate but time consuming. Semi-analytical orbit theory reduces the amount of computer time required for numerical integration of the equations of motion by solving a portion of the equations of motion analytically

(6 and 21). The solution of the filter equations of motion should include semi-analytic orbit theory where applicable.

3. Third-body perturbations due to the sun and moon should be included in the equations of motion to solve the orbit determination problem for high altitude satellites.

4. Different methods of calculating the state transition matrix should be investigated. This should be done in conjunction with suggestion one. Estimating mean orbital elements instead of osculating orbital elements may make the assumption in equation 3.13 more valid.

5. The assumption that the process noise matrix,  $Q$ , and the measurement noise matrix,  $R$ , are diagonal matrices should be relaxed. The effect of off diagonal elements in both matrices should be investigated.

6. Additional tracking data for low, non-circular orbits should be processed to confirm and quantify the precision and advantages of the Gauss filter.

## LIST OF REFERENCES

1. Kolenkiewicz, R. and A. J. Fuchs, "An Overview of Earth Satellite Orbit Determination," AAS 79-107, presented at the AAS/AIAA Astrodynamics Conference, Provincetown, Mass., June 1979.
2. Myers, Filtering Theory Methods and Applications to the Orbit Determination Problem for Near-Earth Satellites, Ph.D. Dissertation, Univ. of Texas at Austin, 1974.
3. NORAD TP SCC 008. Mathematical Foundation for SCC Astrodynamics Theory. Peterson AFB, Colorado: North American Aerospace Defense Command, 1982.
4. Shaver, J. S., Formulation and Evaluation of Parallel Algorithms for the Orbit Determination Problem, Ph.D. Dissertation, Department of Aeronautics and Astronautics, Massachusetts Institute of Technology, Cambridge, Mass., March, 1980.
5. Tapley, B. D. and C. Y. Choe, "Nonlinear Estimation Theory Applied to the Interplanetary Orbit Determination Problem," Third Symposium on Nonlinear Estimation and its Applications, San Diego, Ca., September, 1972.
6. Taylor, S. P. Semianalytic Satellite Theory and Sequential Estimation. Masters Thesis, Department of Aeronautics and Astronautics, Massachusetts Institute of Technology, Cambridge, Mass., September 1981.
7. Athans, Michael, R. P. Wishner, and A. Bertolini, "Suboptimal State Estimation for Continuous-Time Nonlinear Systems from Discrete Noisy Measurements," IEEE Transactions on Automatic Control, Vol. AC-13, No. 5, October, 1968.
8. King-Hele, Desmond. Theory of Satellites in an Atmosphere. London: Butterworth, 1964.
9. Jacchia, L. G. "A Variable Density Model from Satellite Acceleration," Journal of Geophysical Research, Vol. 65, September, 1960.
10. Roy, A. E. Orbital Motion. Bristol: Adam Hilger Ltd., 1982.

11. Merson, R. H. "The Motion of a Satellite in an Axi-Symmetric Gravitational Field," Geophy. J. 4, 17, 1961.
12. Kozai, Y. Smithsonian Institution Astrophysical Observatory Special Report 295, 1969.
13. Kaula, W. M. Theory of Satellite Geodesy. Blaisdell Publ. Co., 1966.
14. Bate, Roger R., Donald D. Mueller, and Jerry E. White. Fundamentals of Astrodynamics. New York: Dover Publications, 1971.
15. Maybeck, Peter S. Stochastic Models, Estimation, and Control. Vol. I, New York: Academic Press, 1979.
16. Maybeck, Peter S. Stochastic Models, Estimation, and Control. Vol. II, New York: Academic Press, 1982.
17. Gelb, Arthur (ED). Applied Optimal Estimation. Cambridge, Massachusetts: The M.I.T. Press, 1974.
18. Jazwinski, Andrew H. Stochastic Processes and Filtering Theory. New York: Academic Press, 1970.
19. Major, Paul E. D06 Technical Note 79-4, Sensor Accuracies. Peterson AFB, Colorado: Aerospace Defense Command, 15 October, 1979.
20. Lawson, Charles L. and Richard J. Hanson, Solving Least Squares Problems. Prentice-Hall, Englewood Cliffs, N.J., 1974.
21. Green, A. J. Orbit Determination and Prediction Processes for Low Altitude Satellites. PhD Dissertation, Department of Aeronautics and Astronautics, Massachusetts Institute of Technology, Cambridge, Mass., December, 1979.
22. Gaposchkin, E. M. and K. Lambeck, "1969 Smithsonian Standard Earth II," S.A.O. Special Report No. 315, 1970.

APPENDIX A  
FUNCTIONS AND COEFFICIENTS FOR TESSERAL HARMONICS

This appendix contains the expressions for the inclination functions and the eccentricity functions found in the tesseral terms in the geopotential as a function of the classical orbital elements, equation 2.17. Also contained in this appendix are the values for the geopotential coefficients  $S_{\ell m}$  and  $C_{\ell m}$ , found in equation 2.17.

Table A-1  
Inclination Functions  $F_{\ell mp}$  (13)

$\ell$	$m$	$P$	$F_{\ell mp}(i)$
2	2	0	$3(1+\cos i)^2/4$
2	2	1	$3\sin^2 i/2$
2	2	2	$3(1-\cos i)^2/4$
3	1	0	$-15\sin^2 i(1+\cos i)/16$
3	1	1	$15\sin^2 i(1+3\cos i)/16-3(1+\cos i)/4$
3	1	2	$15\sin^2 i(1-3\cos i)/16-3(1-\cos i)/4$
3	1	3	$-15\sin^2 i(1-\cos i)/16$
3	2	0	$15\sin i(1+\cos i)^2/8$
3	2	1	$15\sin i(1-2\cos i-3\cos^2 i)/8$
3	2	2	$-15\sin i(1-2\cos i-3\cos^2 i)/8$
3	2	3	$-15\sin i(1-\cos i)^2/8$
3	3	0	$15(1+\cos i)^3/8$

Table A-1 (Continued)

$\ell$	$m$	$P$	$F_{\ell mp}(i)$
3	3	1	$45\sin^2 i(1+\cos i)/8$
3	3	2	$45\sin^2 i(1-\cos i)/8$
3	3	3	$15(1-\cos i)^3/8$
4	1	0	$-35\sin^3 i(1+\cos i)/32$
4	1	1	$35\sin^3 i(1+2\cos i)/16-15(1+\cos i)\sin i/8$
4	1	2	$\cos i(15\sin i/4-105\sin^3 i/16)$
4	1	3	$-35\sin^3 i(1-2\cos i)/16+15\sin i(1-\cos i)/8$
4	1	4	$35\sin^3 i(1-\cos i)/32$
4	2	0	$-105\sin^2 i(1+\cos i)^2/32$
4	2	1	$105(\sin^2 i \cos i(1+\cos i)/8-15(1+\cos i)^2/8$
4	2	2	$105\sin^2 i(1-3\cos^2 i)/16+15\sin^2 i/4$
4	2	3	$-105\sin^2 i \cos i(1-\cos i)/8-15(1-\cos i)^2/8$
4	2	4	$-105\sin^2 i(1-\cos i)^2/32$
4	3	0	$105\sin i(1+\cos i)^3/16$
4	3	1	$105\sin i(1-3\cos^2 i-2\cos^3 i)/8$
4	3	2	$-315\sin^3 i \cos i/8$
4	3	3	$-105\sin i(1-3\cos^2 i+2\cos^3 i)/8$
4	3	4	$-105\sin i(1-\cos i)^3/16$
4	4	0	$105(1+\cos i)^4/16$
4	4	1	$105\sin^2 i(1+\cos i)^2/4$
4	4	2	$315\sin^4 i/8$
4	4	3	$105\sin^2 i(1-\cos i)^2/4$
4	4	4	$105(1-\cos i)^4/16$



Table A-2  
Eccentricity Functions  $G_{\ell pq}(e)$  (13)

1	p	q	1	p	q	$G_{\ell pq}(e)$
2	0	-1	2	2	1	$-e/2$
2	0	0	2	2	0	1
2	0	1	2	2	-1	$7e/2$
2	1	-1	2	1	1	$3e/2$
			2	1	0	1
3	0	-1	3	3	1	$-e$
3	0	0	3	3	0	1
3	0	1	3	3	-1	$5e$
3	1	-1	3	2	1	$e$
3	1	0	3	2	0	1
3	1	1	3	2	-1	$3e$
4	0	-1	4	4	1	$-3e/2$
4	0	0	4	4	0	1
4	0	1	4	4	-1	$13e/2$
4	1	-1	4	3	1	$e/2$
4	1	0	4	3	0	1
4	1	1	4	3	-1	$9e/2$
4	2	-1	4	2	1	$5e/2$
			4	2	0	1

Table A-3  
Tesseral Coefficients (22)

$\ell$	$m$	$C_{\ell m} E-06$	$S_{\ell m} E-06$
2	2	1.5577	-.8806
3	1	2.1277	.4157
3	2	.3047	-.2168
3	3	.0957	.1995
4	1	-.5027	-.4627
4	2	.0738	.1579
4	3	.0591	-.0092
4	4	-.0017	.0072

## APPENDIX B

### STATE TRANSITION MATRIX

The state transition matrix,  $\Phi$ , is used to calculate the linearized observation matrix,  $H$ . Specifically, it is the matrix of partial derivatives of the state vector at some time  $t$  with respect to the state vector at epoch time,  $t_0$ . The method of determining the state transition matrix in this research is based on eq. 3.13:

$$\Phi = I + (t-t_0)F, \quad \text{B-1}$$

where:

$I$  is the identity matrix, and

$F$  is the linearized dynamics matrix.

The linearized dynamics matrix used in the filter equations in Chapter 3 and in equation B-1 to calculate the state transition matrix includes the two-body acceleration, variations due to atmospheric drag, and secular variations due to the zonal terms in the geopotential. The terms in the  $F$  matrix due to two-body acceleration, the tangential component of atmospheric drag, and secular variations due to  $J_2$  are presented in the following equations. All elements of the  $F$  matrix not shown below are zero using this dynamics model.

$$F(1,1) = -nQB\alpha\rho_p \exp(-z) [z(I_1 - I_0) + I_0/2] \quad \text{B-2}$$

$$F(1,2) = nQBza^2\rho_p \exp(-z) [I_0 - I_1]/e \quad \text{B-3}$$

$$F(1,7) = -nQa^2 \rho_p \exp(-z) I_0 \quad B-4$$

$$F(2,1) = -nQB\rho_p \exp(-z) [z(I_0 - I_1) - 1.5I_1] \quad B-5$$

$$F(2,2) = nQB\rho_p \exp(-z) [z(I_1 - I_0) + I_1]/e \quad B-6$$

$$F(2,7) = -nQa\rho_p \exp(-z) I_1 \quad B-7$$

$$F(4,1) = (21/4)J_2(n/a)(R/p)^2 \cos(i) \quad B-8$$

$$F(4,2) = -6nJ_2(R/p)^2 e \cos(i)/(1-e^2) \quad B-9$$

$$F(4,3) = 1.5nJ_2(R/p)^2 \sin(i) \quad B-10$$

$$F(5,1) = (21/4)J_2(n/a)(R/p)^2 (2.5\sin^2(i) - 2) \quad B-11$$

$$F(5,2) = -6nJ_2(R/p)^2 (2.5\sin^2(i) - 2)/(1-e^2) \quad B-12$$

$$F(5,3) = -7.5nJ_2(R/p)^2 \sin(i) \cos(i) \quad B-13$$

$$F(6,1) = -1.5n/a + (21/4)J_2(n/a)(R/p)^2 (1.5\sin^2(i) - 1)(1-e^2)^{1/2} \quad B-14$$

$$F(6,2) = 4.5nJ_2(R/p)^2 (1.5\sin^2(i) - 1)(e/(1-e^2))^{1/2} \quad B-15$$

$$F(6,3) = -4.5nJ_2(R/p)^2 \sin(i) \cos(i) (1-e^2)^{1/2} \quad B-16$$

## APPENDIX C

## SECOND ORDER TERMS FOR FILTER EQUATIONS

The second order filters described in Section 3-4 include terms which require the calculation of the second partial derivatives of the dynamics equations with respect to the state vector at epoch and the second partial derivatives of the observations with respect to the state vector at epoch. This appendix describes the approach used to evaluate these derivatives.

The second partial derivatives of the dynamics equations,  $\underline{f}(\underline{x}, t)$ , with respect to the state vector at epoch,  $\underline{x}(t_0)$ , used to evaluate the dynamic bias term, will be described first. The final result is a set of seven, 7x7 matrices. These seven matrices are evaluated one at a time using the rows from the linearized dynamics matrix,  $F$ , described in Appendix B. The only accelerations needed to calculate the second partial derivatives are the two-body acceleration, the tangential component of the drag acceleration, and the secular component of the acceleration due to oblateness,  $(J_2)$ . The first of the seven matrices, the second partial derivative of the variation in the semi-major axis with respect to the state vector at epoch, is evaluated using row one of the  $F$ -matrix. Similarly, the second partial derivative of the

variation in eccentricity with respect to the epoch state vector is evaluated using the second row of the F-matrix.

It can be immediately observed that the matrices corresponding to the variations in inclination and ballistic coefficient are the null matrices; therefore, the third and seventh elements of the dynamic bias vector will be zero.

The non-zero elements of the seven matrices which represent the second partial derivatives of the dynamics with respect to the state vector at each epoch time are listed below.

Matrix due to variation in semi-major axis:

$$F1(1,1) = nQB\rho_p \exp(-z) [2.0z^2(I_1 - I_0) + I_0(z+1/4)], \quad C-1$$

$$F1(1,2) = -nQB a / e \rho_p \exp(-z) [z(I_1 - I_0) + I_0 e / 2], \quad C-2$$

$$F1(1,7) = -nQ a \rho_p \exp(-z) [z(I_1 - I_0) + I_0 / 2], \quad C-3$$

$$F1(2,1) = F1(1,2), \quad C-4$$

$$F1(2,2) = nQBz(a/e)^2 \rho_p \exp(-z) I_1, \quad C-5$$

$$F1(2,7) = nQza^2 \rho_p \exp(-z) (I_0 - I_1) / e, \quad C-6$$

$$F1(7,1) = F1(1,7), \quad C-7$$

$$F1(7,2) = F1(2,7). \quad C-8$$

Matrix due to variation in eccentricity:

$$F2(1,1) = (n/a)QB\rho_p \exp(-z) [z(2z+3)(I_0 - I_1) - 15I_1]/4, \quad C-9$$

$$F2(1,2) = nQB\rho_p \exp(-z) z(z-1)(I_0 - I_1)/e, \quad C-10$$

$$F2(1,7) = nQ\rho_p \exp(-z) [z(I_1 - I_0) + 1.5I_1], \quad C-11$$

$$F2(2,1) = F2(1,2), \quad C-12$$

$$F2(2,2) = nQB\rho_p \exp(-z) [2z^2(I_0 - I_1) + z(I_0 - 2I_1) - I_1]/e^2, \quad C-13$$

$$F2(2,7) = nQ(a/e)\rho_p \exp(-z) [z(I_0 - I_1) + I_1], \quad C-14$$

$$F2(7,1) = F2(1,7), \quad C-15$$

$$F2(7,2) = F2(2,7). \quad C-16$$

Matrix due to variation in inclination:

$$F3(I,J) = 0.0. \quad C-17$$

Matrix due to variation in ascending node:

$$F4(1,1) = -(189/9)J_2(n/a^2)(R/p)^2 \cos(i), \quad C-18$$

$$F4(1,2) = 21J_2(n/a)(R/p)^2 e \cos(i)/(1-e^2), \quad C-19$$

$$F4(1,3) = -(21/4)J_2(n/a)(R/p)^2 \sin(i), \quad C-20$$

$$F2(2,1) = F4(1,2), \quad C-21$$

$$F4(2,2) = -6J_2 n(R/p)^2 \cos(i) (1+5e^2)/(1-e^2)^2, \quad C-22$$

$$F4(2,3) = 6nJ_2 (R/p)^2 e \sin(i)/(1-e^2), \quad C-23$$

$$F4(3,1) = F4(1,3), \quad C-24$$

$$F4(3,2) = F4(2,3), \quad C-25$$

$$F4(3,3) = 1.5nJ_2 (R/p)^2 \cos(i). \quad C-26$$

Matrix due to variation in argument of perigee:

$$F5(1,1) = -(189/8)J_2 (n/a^2) (R/p)^2 [2.5\sin^2(i)-2], \quad C-27$$

$$F5(1,2) = 21(n/a)J_2 (R/p)^2 e [2.5\sin^2(i)-2]/(1-e^2), \quad C-28$$

$$F5(1,3) = (105/4)J_2 (n/a) (R/p)^2 \sin(i)\cos(i), \quad C-29$$

$$F5(2,1) = F5(1,2), \quad C-30$$

$$F5(2,2) = -6nJ_2 (R/p)^2 [2.5\sin^2(i)-2] (1+5e^2)/(1-e^2)^2, \quad C-31$$

$$F5(2,3) = -30nJ_2 (R/p)^2 e \sin(i)\cos(i)/(1-e^2), \quad C-32$$

$$F5(3,1) = F5(1,3), \quad C-33$$

$$F5(3,2) = F5(2,3), \quad C-34$$

$$F5(3,3) = -7.5nJ_2 (R/p)^2 [\cos^2(i)-\sin^2(i)]. \quad C-35$$

Matrix due to variation in mean anomaly:

$$F6(1,1) = (15/4)n/a - (189/8)J_2 (n/a^2) (R/p)^2 [1.5\sin^2(i)-1] \times (1-e^2)^{1/2}, \quad C-36$$



$$F6(1,2) = -(63/4)(n/a)J_2(R/p)^2[1.5\sin^2(i)-1]e/(1-e^2)^{1/2}, \quad C-37$$

$$F6(1,3) = (63/4)(n/a)J_2(R/p)^2\sin(i)\cos(i)/(1-e^2)^{1/2}, \quad C-38$$

$$F6(2,1) = F6(1,2), \quad C-39$$

$$F6(2,2) = -4.5nJ_2(R/p)^2(1.5\sin^2(i)-1)(1+4e^2)/(1-e^2)^{3/2}, \quad C-40$$

$$F6(2,3) = -13.5nJ_2(R/p)^2\sin(i)\cos(i)e/(1-e^2)^{1/2}, \quad C-41$$

$$F6(3,1) = F6(1,3), \quad C-42$$

$$F6(3,2) = F6(2,3), \quad C-43$$

$$F6(3,3) = 4.5nJ_2(R/p)^2(1-e^2)^{1/2}[\sin^2(i)-\cos^2(i)]. \quad C-44$$

Matrix due to variation in ballistic coefficient:

$$F7(I,J) = 0.0. \quad C-45$$

The other second order terms in the Gauss filter described in Section 3.4 require the calculation of the second partial derivatives of the observations with respect to the epoch state vector. This results in three 7x7 matrices, corresponding to slant range, azimuth, and elevation. These three matrices are used to calculate the bias terms in the observations and the filter gain.

The starting point for calculating the three matrices is the linearized observation matrix, H. The dynamics model described above is used once again. The evaluation of the second partial derivatives would be relatively straightforward; however, the elements of the H-matrix are not available. Instead, the H-matrix is expressed as a product of five matrices:

$$H = M1 \ M2 \ M3 \ M4 \ M5. \quad C-46$$

The approach used is to first evaluate the partial derivatives of H with respect to each of the epoch states. This results in seven 3x7 matrices. The partial derivatives are evaluated using the product rule of differentiation and the chain rule. The first two matrices in equation C-46 are not functions of the epoch state vector; however, the last three matrices are functions of the epoch state vector. The derivatives of the last three matrices in equation C-46 with respect to the elements of the state vector are presented below. The notation used in the following equations is: M3A is the partial derivative of matrix M3 with respect to the semi-major axis, etc.

$$M3A(I,J) = 0.0, \ I=1,...,3; \ J=1,...,7 \quad C-47$$

$$M3E(I,J) = 0.0, \ I=1,...,3; \ J=1,...,7 \quad C-48$$

$$M3I = \begin{bmatrix} \sin\Omega \sin u \sin i & -\cos\Omega \sin u \sin i & \sin u \cos i \\ \sin\Omega \cos u \sin i & -\cos\Omega \cos u \sin i & \cos u \cos i \\ \sin u \cos i & -\cos u \cos i & -\sin i \end{bmatrix} \quad C-49$$

$$M3\Omega = \begin{bmatrix} \sin\Omega \cos u - \cos\Omega \sin u \cos i & \cos\Omega \cos u - \sin\Omega \sin u \cos i & 0 \\ \sin\Omega \sin u - \cos\Omega \cos u \cos i & -\cos\Omega \sin u - \sin\Omega \sin u \cos i & 0 \\ \cos\Omega \sin i & \sin\Omega \sin i & 0 \end{bmatrix} \quad C-50$$

$$M3\omega = \begin{bmatrix} -\cos\Omega \sin u - \sin\Omega \cos u \cos i & -\sin\Omega \sin u + \cos\Omega \cos u \cos i & \cos u \sin i \\ -\cos\Omega \sin u + \sin\Omega \sin u \cos i & -\sin\Omega \cos u - \cos\Omega \sin u \cos i & -\sin u \sin i \\ 0 & 0 & 0 \end{bmatrix} \quad C-51$$

$$M3M = (a/r)^2 (1-e^2)^{1/2} M3\omega. \quad C-52$$

$$M4A(1,2) = (r/a-1)/e, \quad C-53$$

$$M4A(1,6) = e \sin(f) / (1-e^2)^{1/2} - 1, \quad C-54$$

$$M4A(2,4) = (r/a) \cos(i), \quad C-55$$

$$M4A(2,5) = r/a \quad C-56$$

$$M4A(2,6) = (a/r) (1-e^2)^{1/2}, \quad C-57$$

$$M4A(3,3) = (r/a) \sin(u), \quad C-58$$

$$M4A(3,4) = -(r/a) \sin(i) \cos(u). \quad C-59$$

$$M4E(1,1) = k/a, \quad C-60$$

$$M4E(1,2) = k/e - (r-a)/e^2, \quad C-61$$

$$M4E(1,6) = a \sin(f) / (1 - e^2)^{1/2}, \quad C-62$$

$$M4E(2,4) = k \cos(i), \quad C-63$$

$$M4E(2,5) = k, \quad C-64$$

$$M4E(2,6) = a (\cos(f) + ae/r) / (1 - e^2)^{1/2}, \quad C-65$$

$$M4E(3,3) = k \sin(u), \quad C-66$$

$$M4E(3,4) = -k \sin(i) \cos(u), \quad C-67$$

where:

$$k = \partial r / \partial e = -a(2e + e^2 \cos(f) + \cos(f)) / (1 + e \cos(f))^2. \quad C-68$$

$$M4I(2,4) = -r \sin(i), \quad C-69$$

$$M4I(3,4) = -r \cos(i) \cos(u). \quad C-70$$

$$M4\Omega(I, J) = 0.0. \quad C-71$$

$$M4\omega(3,3) = r \cos(u), \quad C-72$$

$$M4\omega(3,4) = r \sin(i) \sin(u). \quad C-73$$

$$M4M(1,1) = k/a, \quad C-74$$

$$M4M(1,2) = k/e, \quad C-75$$

$$M4M(1,6) = (a/r)^2 a e \cos(f), \quad C-76$$

$$M4M(2,4) = k \cos(i), \quad C-77$$

$$M4M(2,5) = k, \quad C-78$$

$$M4M(2,6) = -a \sin(f), \quad C-79$$

$$M4M(3,3) = k \sin(u) - r(a/r)^2 (1-e^2)^{1/2} \cos(u), \quad C-80$$

$$M4M(3,4) = -k \sin(i) \cos(u) + r(a/r)^2 (1-e^2)^{1/2} \sin(i) \sin(u), \quad C-81$$

Where:

$$k = \partial r / \partial M = r \sin(f) / (1 + e \cos(f)). \quad C-82$$

$$M5A(I,J) = F1(I,J) (t-t_0). \quad C-83$$

$$M5E(I,J) = F2(I,J) (t-t_0). \quad C-84$$

$$M5I(I,J) = F3(I,J) (t-t_0) = 0. \quad C-85$$

$$M5\Omega(I,J) = F4(I,J) (t-t_0). \quad C-86$$

$$M5\omega(I,J) = F5(I,J) (t-t_0). \quad C-87$$

$$M6M(I,J) = F6(I,J) (t-t_0). \quad C-88$$

$$M6B(I,J) = F7(I,J) (t-t_0) = 0 \quad C-89$$

The above equations are combined to form the seven 3x7 matrices representing the second partial derivatives of the observations with respect to each state.

$$\partial^2 h / \partial a^2 = M1 \ M2 [M3A \ M4 \ M5+M3 \ M4A \ M5+M3 \ M4 \ M5A], \quad C-90$$

$$\partial^2 h / \partial e^2 = M1 \ M2 [M3E \ M4 \ M5+M3 \ M4E \ M5+M3 \ M4 \ M5E], \quad C-91$$

$$\partial^2 h / \partial i^2 = M1 \ M2 [M3I \ M4 \ M5+M3 \ M4I \ M5+M3 \ M4 \ M5I], \quad C-92$$

$$\partial^2 h / \partial \Omega^2 = M1 \ M2 [M3\Omega \ M4 \ M5+M3 \ M4\Omega \ M5+M3 \ M4 \ M5\Omega], \quad C-93$$

$$\partial^2 h / \partial \omega^2 = M1 \ M2 [M3\omega \ M4 \ M5+M3 \ M4\omega \ M5+M3 \ M4 \ M5\omega], \quad C-94$$

$$\partial^2 h / \partial M^2 = M1 \ M2 [M3M \ M4 \ M5+M3 \ M4M \ M5+M3 \ M4 \ M5M], \quad C-95$$

$$\partial^2 h / \partial B^2 = M1 \ M2 [M3B \ M4 \ M5+M3 \ M4B \ M5+M3 \ M4 \ M5B]. \quad C-96$$

Once the seven 3x7 matrices described above have been calculated, the matrices required for the calculation of the biases in the gain and observations can be determined. The matrix corresponding to the slant range is determined by combining the first rows of the seven 3x7 matrices into a 7x7 matrix. The first row is the first row of equation C-90, the second row is the first row of equation C-91, etc. The matrix corresponding to the azimuth is formulated by using the second rows of the seven matrices described above. Finally, the matrix corresponding to elevation is formulated by combining the last rows of the seven matrices described above.

APPENDIX D  
RADAR SITE LOCATIONS

The locations of the radar sites are provided by SPACECOM/DOA. The components of the site position vectors are defined in terms of a coordinate frame fixed to the Earth with the origin at the center of the Earth. The principal direction,  $\hat{x}$ , is the Greenwich meridian,  $\hat{z}$  is aligned with the North Pole, and  $\hat{y}$  lies in the equatorial plane forming a right handed coordinate frame. The radar site locations used in this research are shown in Table D-1.

Table D-1  
Radar Site Locations

Site Number	X(km)	Y(km)	Z(km)
354	6119.393	-1517.496	-871.566
359	-2382.980	-1420.937	5724.060
363	2881.604	-5372.517	1868.026
393	-3849.481	398.421	5052.965
396	-579.421	-4175.712	4770.682
399	362.839	-5484.293	3225.187

## VITA

Daryl G. Boden was born on May 20, 1949 in Boulder, Colorado. He graduated from Fairview High School in Boulder, Colorado in May 1967. He earned a Bachelor of Science degree in Aerospace Engineering from the University of Colorado in 1972 and a Masters of Science degree in Astronautical Engineering from the Air Force Institute of Technology in 1979. His Air Force assignments include space surveillance officer, astronautical engineer, and ballistic missile systems engineer. He has also served on the faculty of the United States Air Force Academy as an instructor and assistant professor of astronautical engineering.